IEEE Access
Multidisciplinary ⋮ Rapid Review ⋮ Open Access Journal

Received 5 June 2023, accepted 13 June 2023, date of publication 16 June 2023, date of current version 27 June 2023.

Digital Object Identifier 10.1109/ACCESS.2023.3286930

RESEARCH ARTICLE

A Bi-Level Techno-Economic Optimal Reactive Power Dispatch Considering Wind and Solar Power Integration

AAMIR ALI[1,*], GHULAM ABBAS[2,*], MUHAMMAD USMAN KEERIO[1], EZZEDDINE TOUTI[3], ZAHOOR AHMED[4], OSAMAH ALSALMAN[5], AND YUN-SU KIM[6], (Senior Member, IEEE)

[1]Department of Electrical Engineering, Quaid-e-Awam University of Engineering Science and Technology, Nawabshah, Sindh 67450, Pakistan
[2]School of Electrical Engineering, Southeast University, Nanjing 210096, China
[3]Electrical Engineering Department, ENSIT, Laboratory of Industrial Systems Engineering and Renewable Energies, University of Tunis, Tunis 1008, Tunisia
[4]Department of Electrical Engineering, Balochistan University of Engineering and Technology Khuzdar, Khuzdar 89100, Pakistan
[5]Department of Electrical Engineering, College of Engineering, King Saud University, Riyadh 11421, Saudi Arabia
[6]Graduate School of Energy Convergence, Gwangju Institute of Science and Technology (GIST), Gwangju 61005, South Korea

Corresponding author: Yun-Su Kim (yunsukim@gist.ac.kr)

This work was supported by the National Research Foundation of Korea (NRF) grant funded by the Korea government (MSIT) (No. 2022R1C1C1008910).

*Aamir Ali and Ghulam Abbas contributed equally to this work.

ABSTRACT With urban and rural infrastructure development, the power system is being forced to operate at or near its full capacity. This paper proposes four new methodologies to find the solution to the optimal reactive power dispatch (ORPD) problem, considering the capabilities of modern DFIG-based WTs and VSI-based solar PV. The proposed formulation considers the techno-economic objective functions, specifically the minimization of the active and reactive power cost and the maximization of reactive power reserve. This leads to an effective solution to the probabilistic multi-objective ORPD (PMO-ORPD) problem, especially in the context of modern wind farms (WFs) and solar PV. The proposed formulations are necessary for effectively managing power systems with renewable energy sources and contribute to developing efficient and sustainable power systems. Additionally, this study employs probabilistic mathematical modeling that incorporates Weibull, lognormal, and normal probability distribution functions (PDFs) to represent uncertainties in the wind, solar, and load demand. Monte-Carlo simulation (MCS) is employed to generate probabilistic scenarios, allowing for a comprehensive analysis of the PMO-ORPD problem. A new two-phase (ToP) multi-objective evolutionary algorithm is proposed, which incorporates the superiority of feasibility constraints to effectively solve the probabilistic multi-objective optimal reactive power dispatch (PMO-ORPD) problem. From the analysis and comparison of simulation results, it has been observed that the proposed algorithm effectively solves the deterministic and PMO-ORPD problems.

INDEX TERMS Constraint domination principle, multi-objective evolutionary algorithms, optimal reactive power dispatch, reactive power reserve, renewable energy sources.

I. INTRODUCTION

A. LITERATURE REVIEW

The power system is mostly run under stressed operating conditions due to rapid load growth. A rise in greenhouse gas emissions has accompanied the increasing load growth in power systems, a major drawback as more power is required to meet the growing demand and traditional fossil fuel-based power plants are used more frequently, resulting in higher emissions. This has a detrimental environmental impact, contributing to global climate change and other environmental issues. Therefore, power systems need to incorporate clean and sustainable energy sources, such as wind and solar, into their generation mix to mitigate the negative impact of load

The associate editor coordinating the review of this manuscript and approving it for publication was Zhiyi Li.

growth on greenhouse gas emissions. In the atmosphere, they do not impact greenhouse gases like NO_x and SO_x [1]. Alternatively, renewable energy sources (RES), particularly wind and solar, have recently received much attention from academic and industrial circles. As more renewable energy sources, such as solar and wind, are integrated into the power system, managing their variable and intermittent nature has become a major challenge [2]. The power system needs to be flexible enough to accommodate changes in power output and demand and ensure the grid's stability [3].

Furthermore, increasing load demand, i.e., the power system operators (SO), are supposed to move the transmission system with higher loading and lower capacity margin. With the increased loading of the new transmission system, the question of voltage stability is a major concern in the operation of a power system. Voltage stability is a critical aspect of power system operation that refers to the ability of a power system to maintain a steady voltage profile under normal and abnormal operating conditions. Voltage stability is particularly important in load growth, which refers to the increasing demand for electricity in a power system over time [4].

One key factor affecting voltage stability is the system's reactive power level. When a power system experiences a disturbance that causes a change in voltage, reactive power is needed to restore the voltage to its desired level. The voltage may fluctuate or collapse if insufficient reactive power reserve is available in the system, leading to a potential system blackout. Therefore, it is essential to ensure sufficient reactive power reserve in the system to maintain voltage stability during disturbances. This can be achieved by installing reactive power compensation devices such as shunt capacitors, reactors, or operating generators with sufficient reactive power output. Proper voltage control schemes and system planning can also ensure adequate reactive power reserve to maintain voltage stability [5]. Therefore, the availability of a sufficient amount of reactive power supply in the network is thus very critical for the safe and efficient operation of the electrical power system. Voltage stability is a power system's ability to retain appropriate voltages under normal conditions and after a disruption [6]. The SO must also ensure that any contingency or unexpected load variation does not produce a voltage instability that can lead to voltage collapse. Voltage instability point and hence the voltage collapse can be minimized with appropriate availability and distribution of reactive power.

Several scholarly articles have examined the ORDP problem specifically for systems comprised of conventional thermal units using classical optimization techniques such as linear programming (L.P.) [7] and quadratic programming (Q.P.) [8]. These cannot find the global or near-global optimal solution to the ORPD problem. Also, these techniques are implemented to find the solution to the ORPD problem by considering theoretical assumptions such as ORPD is convex, continuous, and differential. With the growing sophistication of computational intelligence, numerous single objective evolutionary algorithms (E.A.s) are being implemented and analyzed for solving non-convex, non-linear ORPD optimization problems considered conventional thermal generators. These include teaching learning-based optimization (TLBO) [9], ant colony optimization [10], quasi-opposition TLBO (QOTLBO) [11], hybrid imperialist competitive algorithm (ICA), and particle swarm optimization (PSO) hybrid ICA-PSO [12], artificial bee colony with firefly (ABC-FF) [13], modified GAME theory [14], quasi-oppositional differential evolution (QODEA) [15] and artificial bee colony (ABC) [5].

Considering only thermal generators to solve the ORPD problem can limit the potential for optimal solutions that balance cost, reliability, and environmental sustainability. Incorporating uncertain renewable resources such as wind and solar generation can provide a more comprehensive and robust approach to power system planning and optimization. Several studies have examined the integration of uncertain load and wind power into the ORPD problem, such as success history-based adaptive differential evolution (SHADE) [16], TLBO [17], and improved marine predator algorithm (IMPA) [18].

In the past few decades, there has been a growing interest in utilizing multi-objective evolutionary algorithms (MOEAs) to efficiently solve MOORPD problems for systems with thermal generators, considering the diverse and complex objectives associated with these systems. That includes non-dominated sorting genetic algorithm II (NSGAII) [19], improved generalized D.E. (I-GDE3) [20], Two-Archive Multi-objective Grey Wolf Optimizer (2ArchMGWO) [21], classification and Pareto domination based MOEA (CPSMOEA) [22], modified NSGAII (MNSGAII) [23], hybrid fuzzy MOEA (HFMOEA) [24], multi-objective Chaotic improved PSO (MOCIPSO) [25], classification and Pareto domination based MOEA (CPDMOEA) [22], multi-objective D.E. (MODE) [26], Chaotic Parallel Vector Evaluated Interactive Honey Bee Mating Optimization (CPVEIHBMO) [27], multi-objective ant lion optimization (MOALO) [28], multi-objective Imperialist Competitive Algorithm (MOICA) [29] and strength Pareto multi-group search optimizer (SPMGSO) [30] were applied to solve MOORPD problems considering conventional thermal generators. In recent years, renewable energy sources such as wind and solar power have become increasingly popular, which poses a challenge for the MOORPD problem due to their uncertain behavior. In the realm of MOORPD problem-solving, incorporating the uncertainty of wind and solar generation has been achieved through the use of optimization techniques such as general algebraic modeling system (GAMS) [31], [32], hybrid artificial physics optimization (APO) and PSO called APO-PSO [33], NSGA-II [34], enhanced firefly algorithm (EFA) [35], opposition-based self-adaptive modified gravitational search algorithm OSAMGSA [36], and two-point estimate method (TPEM) [37]. In these probabilistic MOORPD

problems, reactive power reserve (RPR) was not considered. Reactive power reserve plays a critical role in maintaining stable voltage levels in power systems. Without considering RPR, the system can become unstable and suffer from voltage collapse, leading to power outages, voltage fluctuations, reduce the reliability of the system and increase the risk of blackouts. Neglecting RPR can also reduce the efficiency of the system and increase the operating costs, as maintaining a balance between active and reactive power. Therefore, it is critical to consider RPR in the MOORPD problems to ensure the stable, reliable, and efficient operation of power systems. Stochastic multi-objective optimal dispatch (SMO-OD) [6] were implemented to considered the RPR. However, cost of active power generation were not neglected during optimization. Without proper consideration of the cost of active power, the optimization process may prioritize the reduction of reactive power generation costs at the expense of increased active power generation costs. This can lead to solutions that are not cost-effective and may not meet the economic requirements of the system. The literature review on the ORPD problem is presented in Table 1, which integrates the main findings and limitations of various methodologies used in previous research.

Both wind and solar power generation are probabilistic; due to their high share of these, voltage stability and the expected reactive power reserve (ERPR) can precariously affect them. In addition to the above problems, conventional thermal generators are the key RPR providers in the power system. In recent years, DFIG-based wind turbine (W.T.) and VSI-based solar PV. systems have been able to participate in providing the reactive power reserve (RPR) according to their reactive power capacity curve [40], [41]. The increased integration of wind and solar PV. generation can reduce reactive power generation from conventional thermal generators, increasing the RPR of the system. Maximizing RPR is crucial for maintaining system stability, improving system efficiency, and ensuring the reliable and sustainable operation of the power system [5], [6].

DFIG-based wind farms and VSI-based solar PV. systems are known to have limitations in providing reactive power support to the grid. The electrical system requires reactive power to maintain voltage stability and ensure the system's proper functioning [31]. One of the main challenges with DFIG-based wind farms is their limited capacity to provide reactive power support. This is because the reactive power output of the DFIG is limited by its rotor current and the rotor voltage [40], [41]. As a result, when the wind farm operates at the full reactive power limit, it may not be able to provide sufficient reactive power support to the grid, leading to voltage instability.

Similarly, VSI-based solar PV. systems also have limitations in providing reactive power support. This is because they rely on grid-tied inverters not designed to provide reactive power support [6]. As a result, when the solar PV. system operates at the full reactive power limit, it may not be able to provide sufficient reactive power support to the grid, leading to voltage instability. Operating near the steady-state stability limit can be undesirable because the electrical system operates very close to its maximum capacity, increasing the risk of voltage instability and system failure [32], [36], [37]. Therefore, it is important to ensure that DFIG-based wind farms and VSI-based solar PV. systems are properly synchronized with other reactive power regulators, such as synchronous generators, shunt VAR compensators (SVC), and MVAr injection from the transmission line charging, to maintain voltage stability and ensure the proper functioning of the system [33], [34], [35]. Moreover, both wind and solar power generation are probabilistic. The high share of these sources can lead to voltage instability and a precarious depletion of the expected reactive power reserve (ERPR).

To address these issues, this paper proposed a new methodology to efficiently solve the optimal reactive power dispatch (ORPD) problem, considering modern DFIG-based WTs and VSI-based solar PV. capabilities in the power system. Further, the new techno-economic formulation-based frame resolved not only technical issues (power loss, voltage deviation, and voltage stability index) but also encounter economic issues (cost of active and reactive power, cost of a capacitor, cost of active power loss, and cost of transmission line charging) in the presence of uncertain wind and solar PV. generation. Moreover, the mathematical model of uncertain wind and solar power generation should be properly taken into account to make a realistic technical and economic framework.

B. MOTIVATION

The prime goal of ORPD is to calculate the voltage at PV. buses excluding the slack bus, the transformer's off-nominal turns ratio, and the MVAR injection of SVC. Practically ORPD is a constrained type multi-objective, mixed-integer (transformer turns ratio and SVC are discrete variables), and nonlinear problem. From Table 1, it is concluded that most of the authors considered a conventional ORPD problem to minimize technical single or weighted sum multi-objective function(s) such as minimization of active power loss P_{Loss}, voltage deviation (V.D.), and maximize (VSI) L_{index}. However, in the sense of a deregulated power system, such a formulation seen in the table does not always guarantee that the solution to the problem is appropriate. Therefore, economic objective functions must involve in addition to the technical issues. Some papers in [6], [26], [31], [35], and [38] considered the cost of active or reactive power generation from conventional thermal generators and wind farms. At the same time, the cost of SVC, the effect of MVAr injection from line charging, the cost of power loss, and the combined cost of active and reactive power are not considered. These parameters directly or indirectly affect a power system's reactive power and voltage level. Different models of DFIG-based WFs have been used in the literature, which are limited to either a maximum power factor cos φ or fixed regulation limit [31], [37]. These models are not fully accurate and therefore do not allow the full advantage of the reactive power injection/absorption from the DFIG-based WT.

TABLE 1. Literature review of optimal power dispatch.

Algorithm	Test system	CHT	Objective Function	Problem	Limitations
TLBO [9]	14, 30 & 57-bus	Penalty function	*Cost & P_{Loss}*	Deterministic	Provide a single solution that does not capture the trade-offs between different objectives. It cannot lead to more informed and robust decision-making. The cost of active power generation was neglected, leading to increased operating costs, inefficient allocation of resources, and not being suitable for long-term planning. Wind or solar integration was not studied as wind and solar energy sources became more prevalent.
ACO [10]	I57 & 118	Penalty function	*P_{LOSS}, and VSI*	Deterministic	
QOTLBO [11]	30 & 118	Penalty function	*P_{LOSS}, V.D., and VSI*	Deterministic	
ICA-PSO [12]	57 & 118-bus	Penalty function	*P_{Loss} & VD*	Deterministic	
ABC-FF [13]	14 & 39-Bus	Penalty function	*P_{Loss} & VD*	Deterministic	
GAMS [14]	39-bus	ECM, WS & GP	*P_{Loss} & VD*	Deterministic	
QODEA [15]	30, 57 & 118-bus	Penalty function	*P_{LOSS}, V.D., and VSI*	Deterministic	
ABC [5]	30, 508-bus	Penalty function	*P_{Loss}, VD, and RPR*	Deterministic	
SHADE [16]	*30 & 57-bus.*	ECM	*P_{Loss} & VD*	Probabilistic	Without sufficient reactive power reserve, the system may experience voltage instability, leading to voltage fluctuations, equipment damage, power outages, and even blackouts.
TLBO [17]	30 &118-bus	Linearization	*P_{LOSS}, V.D.*	Probabilistic	
IMPA [18]	30	Penalty function	*P_{LOSS}, V.D. & VSI*	Probabilistic	
ECM [38]	30-bus	ECM	*SVCs, P_{LOSS}, VSI*	Probabilistic	
NSGA-II [19]	118	Penalty function	*P_{Loss} & VD*	Deterministic	Wind and solar integration were not implemented, and missed opportunities for realizing the benefits of renewable energy sources. Inaccurate system modeling, inefficient use of resources, reduced reliability, poor future planning. RPR was not studied, which can lead: to voltage instability, inefficient use of resources, inability to handle unexpected events, and increased risk of equipment damage.
I-GDE3 [20]	118 & 300-Bus	Penalty function	*P_{Loss} & VD*	Deterministic	
2ArchMGWO [21]	30, 57 & 118-bus	Penalty function	*P_{LOSS} & VD*	Deterministic	
CPSMOEA [22]	30 & 118	Penalty function	*P_{Loss} & VD*	Deterministic	
MNSGA-II [23]	30 & 118	Feasibility rule	*P_{LOSS}, and VSI*	Deterministic	
HFMOEA [24]	24 RTS	Feasibility rule	*P_{LOSS}, and VSI*	Deterministic	
MOCIPSO [25]	30 and 57	CPR	*P_{LOSS}, and VSI*	Deterministic	
CPSMOEA [22]	30 & 118-bus	Penalty function	*P_{Loss} & VD*	Deterministic	
MODEA [26]	30 & 57-Bus	Penalty function	*I.C., P_{LOSS} & VSI*	Deterministic	
NSGA-II [39]	30-bus	WSA	*P_{Loss} & VD*	Deterministic	
CPVEIHBMO [27]	30, 57 & 118	Penalty function	*P_{LOSS}, V.D., and VSI*	Deterministic	
MOALO [28]	30, 57 & 300-bus	FR	*P_{LOSS}, VD and VSI*	Deterministic	
MOICA [29]	30, 57 & 118 bus	CDP	*P_{LOSS}, VD and VSI*	Deterministic	
SPMGSO [30]	30 & 162	Penalty function	*P_{LOSS}, V.D., and VSI*	Deterministic	
TPEM [37]	14 & 30 Bus	WSA	*P_{Loss} & VD*	Probabilistic	RPR was not implemented, which can lead: to voltage instability, inefficient use of resources, poor integration of renewable energy sources, inability to handle unexpected events, and increased risk of equipment damage.
NSGA-II [34]	30-bus	ECM	*P_{Loss} & VD*	Probabilistic	
GAMS [32]	57-bus	ECM & FSA	*P_{LOSS}, and VSI*	Probabilistic	
APO-PSO [33]	30, 57 & 118 bus	Penalty function	*P_{LOSS}, V.D., and VSI*	Probabilistic	
OSAMGSA [36]	30-Bus	Penalty function	*P_{LOSS}, V.D., and VSI*	Probabilistic	
GAMS [31]	30 & 118	ECM	*P_{Loss}, Cost of WT, VSI*	Probabilistic	
EFA [35]	30	Penalty function	*P.L., V.D. & cost of M.W.*	Probabilistic	
SMO-ODC [6]	30-bus	ECM	*Cost of MVAr & RPR*	Probabilistic	Does not consider the cost of reactive power can lead to increased costs, inefficient use of resources, poor allocation of resources, and reduced competitiveness.

CHT=Constraint Handling Technique, FR=Feasibility rule, WSA=weighted sum approach, ECM=epsilon constraint method, O&M=Operation, and maintenance cost, P_{Loss}=Active power loss, IC=Cost of SVC, CDM=constraint domination principle, VSI=voltage stability index (L_{index}), VD=Voltage deviation, OAPD=Optimal active power dispatch, FSA=Fuzzy selection approach, CPR= constrain-prior method

C. CONTRIBUTION

The optimization of active and reactive power generating costs and the maximizing of reactive power reserve (RPR) were taken into consideration in a few articles that solved deterministic and probabilistic single objective ORPD problems. The authors have conducted a literature review and found that no previous studies have considered a PMO-ORPD problem that simultaneously incorporates techno-economic objective formulations, including the cost of active and reactive power, as well as Reactive Power Reserve (RPR) and L_{index}, in the presence of Doubly-Fed Induction Generator (DFIG)-based Wind Turbines (W.T.) and Voltage-Source Inverter (VSI)-based solar Photovoltaic (PV.) systems. Also, research on managing the RPR generated by the DFIG-based WT and VSI-base solar PV. system with the maximization of RPR of thermal generators has not yet been examined. In the proposed formulation, the two main objective functions are the minimization of the expected cost of reactive power-producing devices and the maximization of expected RPR (ERPR). Four new formulations are modeled for deregulated power systems to solve the PMO-ORPD problem focusing on system voltage security. For a realistic system, 1000 scenarios are generated using the active power of wind, solar PV., and variable load demand then the fuzzy C-means

(FCM) clustering technique is applied to find the 20 representative scenarios. The multi-objective problem is solved using a constrained two-phase (ToP) algorithm that computes the number of non-dominated solutions (Pareto Front) for the system operator in a single simulation run.

The best compromise solution from the non-dominated solution is computed with the help of fuzzy decision-making (FDM) theory. The main contributions of this work are detailed as follows:

- A new probabilistic multi-objective optimal reactive power dispatch (PMO-ORPD) model is proposed, which considers the integration of DFIG-based WT and VSI-based solar PV. and considers techno-economic objective functions.
- The proposed PMO-ORPD model is solved using a new two-phase (ToP) multi-objective evolutionary algorithm (MOEA) that integrates the superiority of feasibility constraint handling to solve the ORPD problem efficiently.
- Incorporated appropriate probability distribution functions (PDFs) to model the probabilistic wind and solar generation and applied a Fuzzy C-means (FCM) clustering technique to extract the most representative scenarios to reduce the problem's computational complexity.
- The proposed algorithm has been compared to various recent constrained multi-objective evolutionary algorithms (CMOEAs) that have not been previously employed to solve the classical ORPD problem.

The remaining sections of the paper are divided as follows. The MO-ORPD problem is formulated in Section II, which involves uncertain generation and demand modeling, formulation of objective functions, and constraints. Section III deliberates the proposed algorithm. Section IV provides the investigation of simulation results. Section V gives the discussion, and Section VI elucidates the conclusion of this work.

II. PROBLEM FORMULATION

In the following subsections, PDFs of wind solar and load demand are modeled. Next, modeling the reactive power capability curve of DFIG-based Wind and VSI-based solar PV. was discussed. The operating cost of active and reactive power is computed in this section. Two classical formulations based on objective technical functions and four new formulations based on techno-economic formulation are modeled. The decision variables, multi-objective functions, and operational constraints are formulated.

A. MODELING OF UNCERTAIN LOAD DEMAND, WIND, AND SOLAR GENERATION

In the literature, load demand, wind, and solar power generation have all been modeled using normal, Weibull, and lognormal PDFs [6]. The PDFs mentioned above are mathematically defined as:

Weibull PDF for the wind velocity (v) estimating:

$$\Delta_v(v) = \left(\frac{b}{a}\right)\left(\frac{v}{a}\right)^{(b-1)} \times e^{\left[-\left(\frac{v}{a}\right)^b\right]} \tag{1}$$

Lognormal PDF for the solar irradiance (G) predicting:

$$\Delta_G(G) = \frac{1}{G \times d\sqrt{2\pi}} e^{\left[\frac{-(lnG-c)^2}{2d^2}\right]} \tag{2}$$

Active and reactive load demand (l) is modeled as;

$$\Delta_D(l) = \frac{1}{\sigma\sqrt{2\Pi}} \times e^{-\left(\frac{(l-\mu)^2}{2\sigma^2}\right)} \tag{3}$$

Δ shows probability; a, b, c, d μ, and σ are the standard parameters of Weibull, lognormal and normal PDF are given in Table 9 in an appendix. Wind power is the function of wind velocity (v) and is calculated as [34]:

$$p_{gW}(v) = \begin{cases} 0, for\, v < v_{in}\ and\ v > v_{out} \\ P_{wr}\left(\dfrac{v - v_{in}}{v_r - v_{in}}\right) for\ v_{in} \le v \le v_r \\ P_{wr}\ for\ v_r < v \le v_{out} \end{cases} \tag{4}$$

whereas the parameters v_{in}, v_r and v_{out} are the cut-in, rated, and cut-out wind speeds. Solar power (p_{gS}) is the function of solar irradiance and is calculated as [34]:

$$p_{gS}(G) = \begin{cases} P_{sr}\left(\dfrac{G^2}{G_{sTd}R_c}\right) for\ 0 < G < R_c \\ P_{sr}\left(\dfrac{G}{G_{sTd}}\right) for\ G \ge R_c \end{cases} \tag{5}$$

where G_{std} and R_c are the solar irradiances and certain irradiance at 1000 W/m^2 and 120 W/m^2, respectively, figure 1 shows the generation of normal, Weibull, and lognormal PDFs considering 1000 Monte Carlo simulation (MCS) states. Parameters for the generation of probabilistic scenarios of load, wind, and solar PV. generation are reported in Appendix Table 9.

For a given scenario, the computation of the objective functions of a candidate planning will pose a heavy computational burden in the optimization process. Therefore, a clustering approach, which can reduce the computational burden by eliminating identical scenarios, is employed to find the representative scenarios. This paper applies a fuzzy C-means clustering method to find the 20 representative scenarios. In this method, all 1000 MCS load, wind, and solar PV. power scenarios are initially normalized between 0 and 1. Then, it is possible to further divide each normalized variable into a specified number of clusters. Through this, it is possible to generate the total number of possible representative clusters/scenarios N_{sc} and their associated probability ρ_{sc}. For detail, see *fcm* built-in MATLAB function for computing representative scenarios and their probability.

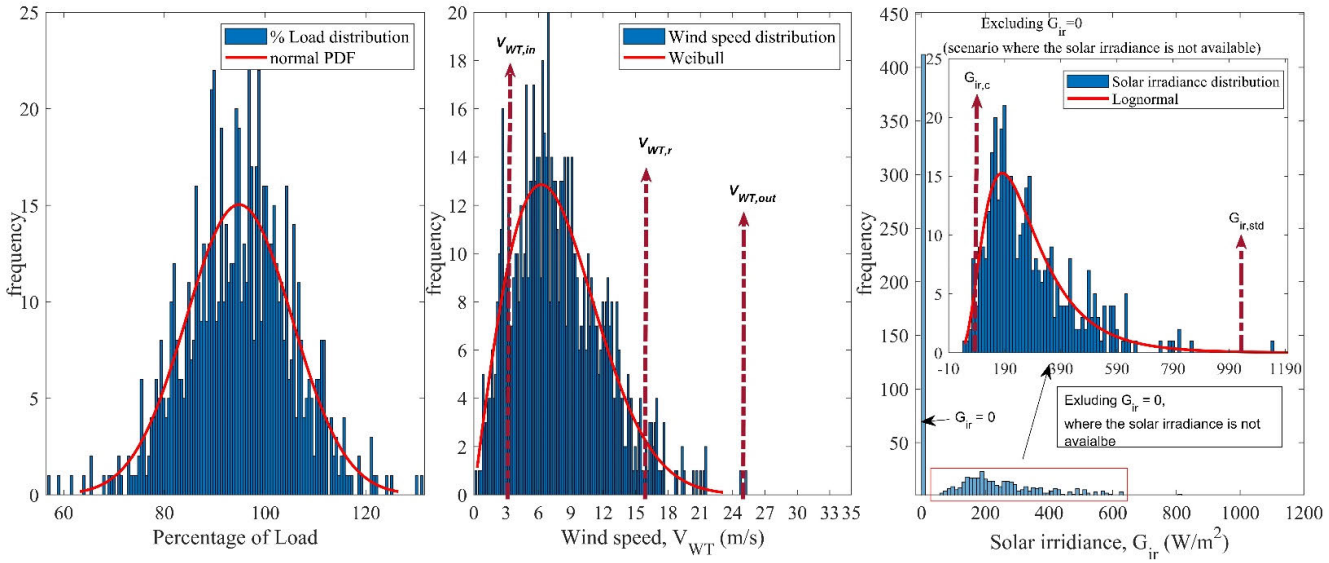

FIGURE 1. PDF functions of wind, solar, and load demand considering 1000 samples of MCS.

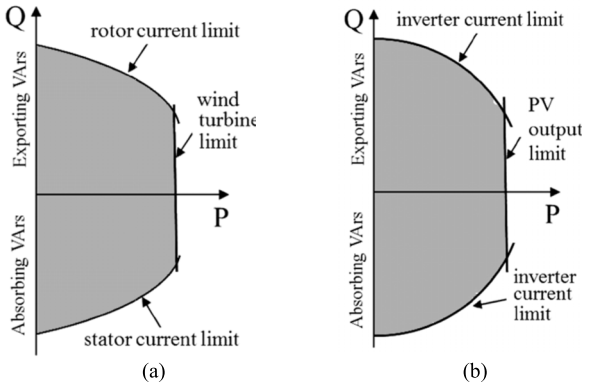

FIGURE 2. Reactive power Capability curve a) DFIG-based wind and b) VSI-based solar PV. [41].

B. MODELING OF REACTIVE POWER CAPABILITY LIMIT FOR WIND AND SOLAR PV SYSTEMS

In the literature, wind and solar usually inject active power into the system. Whereas, the reactive power from these sources can be injected into the system, which helps to strengthen the voltage profile, and RPR and minimize energy loss. The lack of attention at the planning stage to the reactive power injection/absorption by Wind and solar PV. generation units could contribute to a possible rise in investment costs. Therefore, this paper integrates renewable energy source technologies, including DFIG-based WT and VSI-based solar PV. with the system. The reactive power capability constraints of these probabilistic sources shown in Fig. 2 are discussed below.

1) DFIG-BASED WT

Maximum reactive power absorption/injection of DFIG-based WT depends on the slip (s) and probabilistic active power generation ($p_{gW,sc}$), whereas active power is the function of wind speed (v). From Figure 2 (a), it is clearly showing that the maximum reactive power absorption or injection $Q_{i,sc}^{w,absorb}$ /$Q_{i,sc}^{w,inject}$ depends on the stator/ rotor current limit I_i^{scwd}/ I_i^{scwd}, respectively. Mathematically, $Q_{i,sc}^{w,absorb}$/$Q_{i,sc}^{w,inject}$ can be computed as [41]

$$Q_{i,sc}^{w,absorb} = -\sqrt{\left(|V_{i,sc}|\, I_i^{scwd}\right)^2 - \left(\frac{p_{gW,sc}}{1-s_{sc}}\right)^2} \tag{6}$$

$$Q_{i,sc}^{w,inject} = \frac{|V_{i,sc}||Z_i^m| I_i^{rcwd} sin\gamma_{i,sc}}{|Z_i^s + Z_i^m|} - \frac{|V_{i,sc}|^2 (X_n^s + X_n^m)}{|Z_i^s + Z_i^m|^2} \tag{7}$$

where $V_{i,sc}$ is the system voltage at bus i over a scenario (sc) and $s_{i,sc}$ is the slip of a DFIG-based wind unit at a scenario (sc). $Z_i^m = R_i^m + jX_i^m$ and $Z_i^s = R_i^s + jX_i^s$ are the equivalent main and stator impedances respectively of W.T. Power factor angle $\gamma_{i,sc}$ is given as

$$\gamma_{i,sc} = cos^{-1}\left(\frac{P_{n,sc}^{wd}|Z_i^s + Z_i^m|^2 + |V_{i,sc}|^2\left(R_i^s + R_i^m\right)}{\left(1 - s_{i,st}\right)|V_{i,st}||Z_i^m||Z_i^s + Z_i^m| I_i^{rcwd}}\right) \tag{8}$$

2) VSI-BASED SOLAR PV

Figure 2 (b) clearly shows that the maximum absorption/ injection (reactive power capability limit) of VSI-based solar PV. depends on the inverter current limit $I_i^{pv,in}$ [5]. Maximum and minimum reactive capability limits of VSI-based solar PV. can be computed as

$$Q_{i,sc}^{pv,max}, Q_{i,sc}^{pv,min} = \pm\sqrt{(|V_{i,sc}| I_i^{pv,in})^2 - (p_{gS,sc}(G))^2} \tag{9}$$

Parameters for the computation reactive power limit, for both wind and solar PV. generation, are given in Table 12 of the Appendix.

C. OBJECTIVE FUNCTIONS AND CONSTRAINTS

1) CLASSICAL FORMULATION

In the literature, expected P_{Loss} (EP_{Loss}), expected V.D. (EVD), and expected L_{index} (EL_{index}) [5] objective functions are used for deterministic and probabilistic ORPD problems. These objective functions can be calculated as:

$$EP_{Loss} = \sum_{sc=1}^{Nsc} \times \rho_{sc} \left(\sum_{k=1}^{nl} G_{k(ij)}[V_i^2 + V_j^2 - 2V_iV_jcos(\delta_{ij})] \right) \quad (10)$$

$$EVD = \sum_{sc=1}^{Nsc} \rho_{sc} \left(\sum_{L=1}^{NL} |V_L - 1| \right) \quad (11)$$

$$EL_{index} = \sum_{sc=1}^{Nsc} \rho_{sc} \times L_{index,sc} \quad (12)$$

whereas k is the branch connecting i and j sending and receiving end buses, Nsc is the total number of representative scenarios, $G$is branch conductance, δ voltage angle, $N_{.L.}$ is the load buses. EL_{index} indicator [5] has developed on L_j local indicator. Let $N.G.$and $N.L.$ be the number of generator and load buses, respectively, then local indicator L_j can be calculated as;

$$L_j = \left| 1 - \sum_{i=1}^{GN} F_{ji} \frac{V_i}{V_j} \right|, where\ j = 1, 2, \ldots, NL \quad (13)$$

$$L_{index} = min\left(max\left(L_j\right)\right) \quad (14)$$

where , $F_{ji} = -[Y_{LL}]^{-1}[Y_{LG}]$ and Sub-matrices Y_{LL} and Y_{LG} are calculated from the Y_{BUS} matrix after separating PV. and P.Q. buses.

This paper considers two classical formulations, the optimization of technical objective functions,. These are,

- Classical formulation, C1: simultaneous minimization of EP_{Loss} and EVD
- Classical formulation, C2: simultaneous minimization of EP_{Loss} and EL_{index}

C1 and C2 are both available in the literature.

2) PROPOSED FORMULATION

The system voltage level affects active and reactive power losses in a power system. Therefore, operational cost is the total cost incurred by the system to maintain the given thermal generator capacity, L_{index}, and voltage level. Renewable energy generation, however, is seasonal and varies depending on the circumstance. Therefore, this paper aims to find the solution to the PMO-ORPD problem so that the expected RPR (ERPR) is maximized along with the minimization of the expected energy cost. Technically, it can be said that the system's reactive power and voltage profile depend on each other. Therefore, in the proposed formulation, ERPR is maximized. Here, the authors proposed various formulations of simultaneously 2 and 3 objective functions. For each proposed formulation operating cost of reactive power includes the cost of reactive power, the cost of active power loss, the cost of shunt capacitors, and the cost of reactive injection from line charging. Mathematically expected total operating cost (ETC_t) is computed as:

$$ETC_t = \sum_{sc=1}^{Nsc} \rho_{sc} \times \sum_{G=1}^{N_G} \left(C_{P_{G,s\,c}} + C_{Q_t} + C_{L_t} \right) \quad (15)$$

where, N_G, N_C and N_{Ch} are the total number of generators, shunt condensers, and transmission line that injects reactive power from line charging, respectively, P_{GL_i} is the total amount of active power loss allocated to the ith generator for the whole system and P_{G_i} is the amount of power supplied by ith generator. From (15), C_{P_G} and C_{Q_t} are the total active and reactive power costs and C_{L_t} is system active power loss cost in \$/h. These can be defined as:

$$C_{P_G} = a_iP_{G_i}^2 + b_iP_{G_i} + c_i \quad (16)$$

$$C_{Q_t} = \sum_{G=1}^{N_G} C_{Q_{G,s\,c}} + \sum_{c=1}^{N_C} C_{Q_{C,s\,c}} + \sum_{ch=1}^{N_{ch}} C_{Q_{ch,,s\,c}} \quad (17)$$

$$C_{Q_G} = \sum_{G=1}^{N_G} a_QQ_{G_i}^2 + b_QQ_{G_i} + C_Q \quad (18)$$

$$C_{Q_C} = \$\,0.1324 \cdot Q_{Cap}/MVAr - hr \quad (19)$$

$$C_{Q_{Ch}} = c_{ch} \cdot Q_{Ch} \quad (20)$$

$$Q_{ch} = \sum_{ij=1}^{N_{br}} Q_{C_{i-j}} \quad (21)$$

$$Q_{C_{i-j}} = V_i^2\frac{y_{C_{ij}}}{2} + V_j^2\frac{y_{C_{ij}}}{2} \quad (22)$$

where a_Q, b_Q, c_Q are the cost coefficients determined from the active power cost coefficients a_i, b_i, c_i [42] and C_{Q_C} is the cost of synchronous condenser, Q_{Cap} is the decision variable between 0 to 5 MVAr, c_{ch} is the reactive power per unit cost supplied by transmission line charging. $Q_{C_{i-j}}$ is computed after the load flow by knowing the voltage at from V_i and to V_j bus,$Y_{C_{ij}}$ is the line charging admittance of pi transmission line,N_{br} are the total number of lines.

The expected cost of total reactive power can be calculated as

$$ETC_{Q_t} = \sum_{sc=1}^{Nsc} \rho_{sc} \times C_{Q_t} \quad (23)$$

In this paper, the cost of active power loss C_{L_t} is computed by using Pro Rata Allocation (PRA) [43]method.

$$C_{L_t} = \sum_{i=1}^{NG} \left(\left(a_iP_{G_i}^2 + b_iP_{G_i} + c_i \right) K_G \right) \quad (24)$$

where K_G is the Loss allocation factor (LAF) for the generator at bus i. For the computation of LAF, PRA method proportionally allocates 50% of losses to the generators, that is,

$$K_G = \frac{1}{2}\frac{P_{Tloss}}{P_G} \quad (25)$$

where, P_G is the total amount of active power generation and P_{Tloss} is the total active power loss. It should be noted that generation loss allocation factors K_G are identical for all buses. Additionally, it should be noted that losses allocated to generators are always positive. The expected reactive power

reserve (ERPR) at the scenario (sc) is expressed as follows

$$ERPR = \sum_{sc=1}^{N_{sc}} \left(\rho_{sc} \sum_{G=1}^{N_G} \left(Q_{G_i}, sc^{max} - Q_{G_i}, sc \right) \right) \tag{26}$$

The following PMO-ORPD objective function formulation has been proposed considering the techno-economic objective functions.

- Formulation 1— minimization of ETC_{Q_t} vs maximizes the $ERPR$
- Formulation 2— minimize the ETC_t vs maximizes the $ERPR$
- Formulation 3— minimization of ETC_{Q_t} vs maximizes the $ERPR$ along with maximizing Q_{ch}
- Formulation 4 — minimization of ETC_{Q_t} vs maximizes the $ERPR$ along with maximizing Q_{ch} vs EL_{index}

Coefficients for calculating the cost of active and reactive power are given in Table 11 of the Appendix.

3) DECISION VARIABLES AND CONSTRAINTS

Multi-objective functions are given as:

$$\begin{aligned} &\min \mathbf{F}\left(\vec{x}\right) = \left[f_1\left(\vec{x}\right), f_2\left(\vec{x}\right), \ldots, f_M\left(\vec{x}\right)\right]; \\ &s.t \phi\left(\vec{x}\right) = 0, \psi(\vec{x}) \leq 0 \end{aligned} \tag{27}$$

Vector $\mathbf{F}\left(\vec{x}\right)$ is the objective function, $\phi\left(\vec{x}\right)$ are the equality constraints and $\psi(\vec{x})$ are inequality constraints. The decision variable $\vec{x}$ is defined as;

$$\vec{x} = \left[\underbrace{[V_{G,1}, \cdots, V_{G,N\ G}}_{V_G}, \underbrace{Q_{c,1}, Q_{c,N\ C}}_{Q_c}, \underbrace{T_{k,1}, T_{k,N\ T}}_{T_k}]^T \right] \tag{28}$$

where $N.G.$, NC, and $N.T.$ are the network's total numbers of generators, synchronous condensers, and transformers. In the proposed formulation, active and reactive power balance constraints are computed as

$$P_{G_i} - P_{D_i} = V_i \sum_{j=1}^{NB} V_j \left[G_{ij}\, cos\left(\delta_{ij}\right) - B_{ij}\, sin\left(\delta_{ij}\right) \right] \tag{29}$$

$$Q_{G_i} - Q_{D_i} = V_i \sum_{j=1}^{NB} V_j \left[G_{ij}\, sin\left(\delta_{ij}\right) - B_{ij}\, cos\left(\delta_{ij}\right) \right] \tag{30}$$

whereas G_{ij} and B_{ij} are the conductance and susceptance of transmission lines, P_{Di} and Q_{Di} are the real and reactive power demand. On the other hand, inequality constraints are.

$$V_L^{min} \leq V_L \leq V_L^{max} \tag{31}$$

$$V_G^{min} \leq V_G \leq V_G^{max} \tag{32}$$

$$P_G^{min} \leq P_G \leq P_G^{max} \tag{33}$$

$$Q_G^{min} \leq Q_G \leq Q_G^{max} \tag{34}$$

$$T_j^{min} \leq T_j \leq T_j^{max}\ \forall j \in NT \tag{35}$$

$$Q_c^{min} \leq Q_c \leq Q_c^{max} \tag{36}$$

$$S_l \leq S_l^{max} \tag{37}$$

V_L is the Voltage at the load bus, V_G voltage PV. bus, $P_G$and Q_G are the active and reactive power of generators, T_j is the transformer tapings, Q_c is the MVAr capacity of SVC and S_l is the MVA branch flow limit. This paper considers the base configurations of the IEEE 30-bus systems to perform deterministic ORPD and compare the results with previously published studies. All thermal generators are included in the base designs. For stochastic ORPD, a DFID-based wind generator and a VSI-based solar PV. are integrated into the IEEE 30-bus system. Specifically, a wind power generating source replaces the thermal generator at bus 5, while a photovoltaic power plant replaces the thermal generator at bus 8. The modified system's diagram is illustrated in Figure 3.

III. CONSTRAINED TWO-PHASE (ToP) ALGORITHM

The paper focuses on optimizing multiple objectives including the cost of reactive power injection, RPR, VD, P_{Loss}, and L_{index}, which makes the problem more complex due to the addition of constraints. This complexity makes it difficult for a multi-objective evolutionary algorithm (MOEA) to identify promising feasible solutions for the PMOORPD problem efficiently. Since a constrained MOEA must balance all the objective functions within the feasible region, the convergence speed of the population is unavoidably slow. To address this issue, the proposed algorithm first aims to identify high-quality feasible solutions as

$$minF\left(x\right) = \frac{1}{m} \sum_{i=1}^{m} f_i\left(x\right) \tag{38}$$

where m is the number of objective functions. The primary aim of the first phase is to offer high-quality feasible solutions for the subsequent phase. Additionally, the search engines for producing offspring utilize two well-known trail vector strategies of differential evolution (D.E.). These strategies are

D.E./current-to-rand/l

$$\vec{u}_i = \vec{x}_i + F * (\vec{x}_{r1} - \vec{x}_i) + F * (\vec{x}_{r2} - \vec{x}_{r3}) \tag{39}$$

D.E./rand-to-best/l/bin

$$\vec{v}_i = \vec{x}_{r1} + F * (\vec{x}_{best} - \vec{x}_{r1}) + F * (\vec{x}_{r2} - \vec{x}_{r3}) \tag{40}$$

$$\vec{u}_{i,j} = \begin{cases} \vec{v}_{i,j}\ if\ rand_j < CR\ or\ j = j_{rand} 1, \ldots, D \\ \vec{x}_{i,j}\ otherwise \end{cases} \tag{41}$$

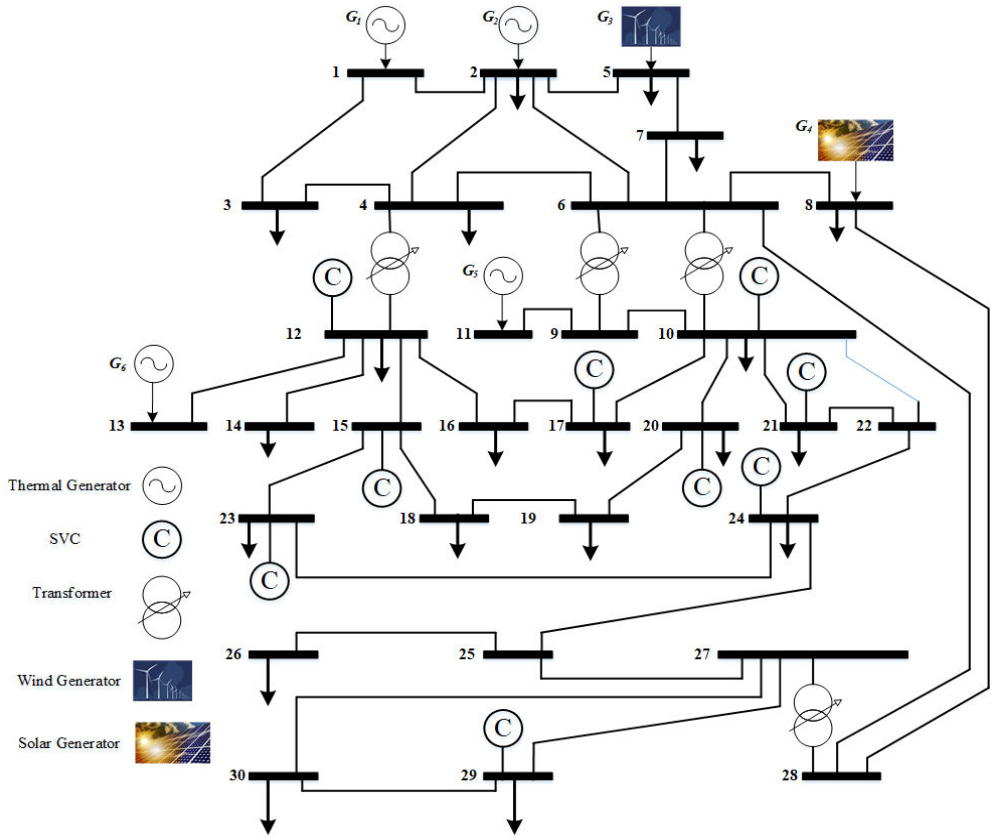

FIGURE 3. Proposed IEEE 30-bus system with a wind generator and a photovoltaic unit.

where, subscript $i \in [1, Np]$ and $j \in [1, D]$; D is the decision vector; $v_i = (v_{i,1}, v_{x,2}, \ldots, v_{i,D})^T$ is the i^{th} mutant vector; $u_i = (u_{i,1}, u_{i,2}, \ldots, u_{i,D})^T$ is the i^{th} trial vector; r_1, r_2 and r_3 are random integers between $[1, Np]$, $\vec{x}_{\text{best}}$ is the best individual in the current population, $rand_j$ arbitrary number [0, 1], j_{rand} is a random number $[1, D]$, F and CR are the scaling and crossover control parameters, and these are randomly selected from the $\text{F}_{\text{pool}} = [0.6; 0.8; 1.0]$ and $\text{CR}_{\text{pool}} = [0.1; 0.2; 1.0]$.

The feasibility rule constraint technique is utilized to determine the superior solution between the $\vec{x}_i$ and $\vec{u}_i$ for the next generation. It is imperative to terminate the first phase once high-quality solutions have been achieved, even if the entire population has not converged to a single point. To accomplish this, the following two conditions are established:

Condition 1: The feasibility proportion (Pf) should be greater than 1/3, ensuring the feasible region has been reached.

Condition 2: The normalized weighted sum of single objective functions $\tilde{f}(\vec{x})$ is calculated and added together.

$$\tilde{f}_i(\vec{x}) = \frac{f_i(\vec{x}) - f_{min}(\vec{x})}{f_{max}(\vec{x}) - f_{min}(\vec{x})} \tag{42}$$

$$\overline{f}(\vec{x}) = \sum_{i=1}^{m} \tilde{f}_i(\vec{x}) \tag{43}$$

Next, the values of $\overline{f}(\vec{x})$ are sorted, and the largest difference (δ) is computed for the top 33% of feasible solutions. If δ is less than 0.2, the second condition is met, indicating that some high-quality solutions have been obtained and are converging to smaller regions. The primary objective of the first phase is to generate high-quality solutions for the subsequent phase. However, the solutions obtained may not be well-distributed or effectively converged. Thus, in the second phase, a popular MOEA, namely the non-dominated sorting genetic algorithm (NSGAII) along with the domination rule of (SPEA2) [44], is employed to obtain a well-distributed and global Pareto front. Each population in this dominance rule assigns a fitness value based on the quantity of dominated solutions. Less fitness will be associated with a solution if it dominates a large number of other solutions, and vice versa. After that, fitness values are taken into account when utilizing a tournament selection operator to choose the mating pools (parents) of each population.

Then, a simulated binary crossover operator is applied between randomly selected parents from the mating pool to create child populations for better exploitation. On the other hand, the polynomial mutation operator is applied to increase the exploitation of the capability of the proposed algorithm. The combined population and offspring's updated fitness values (i.e., fitness) are then computed. Finally crowding distance operator is applied to select the final survival of the fittest population for the next generation. The procedure as

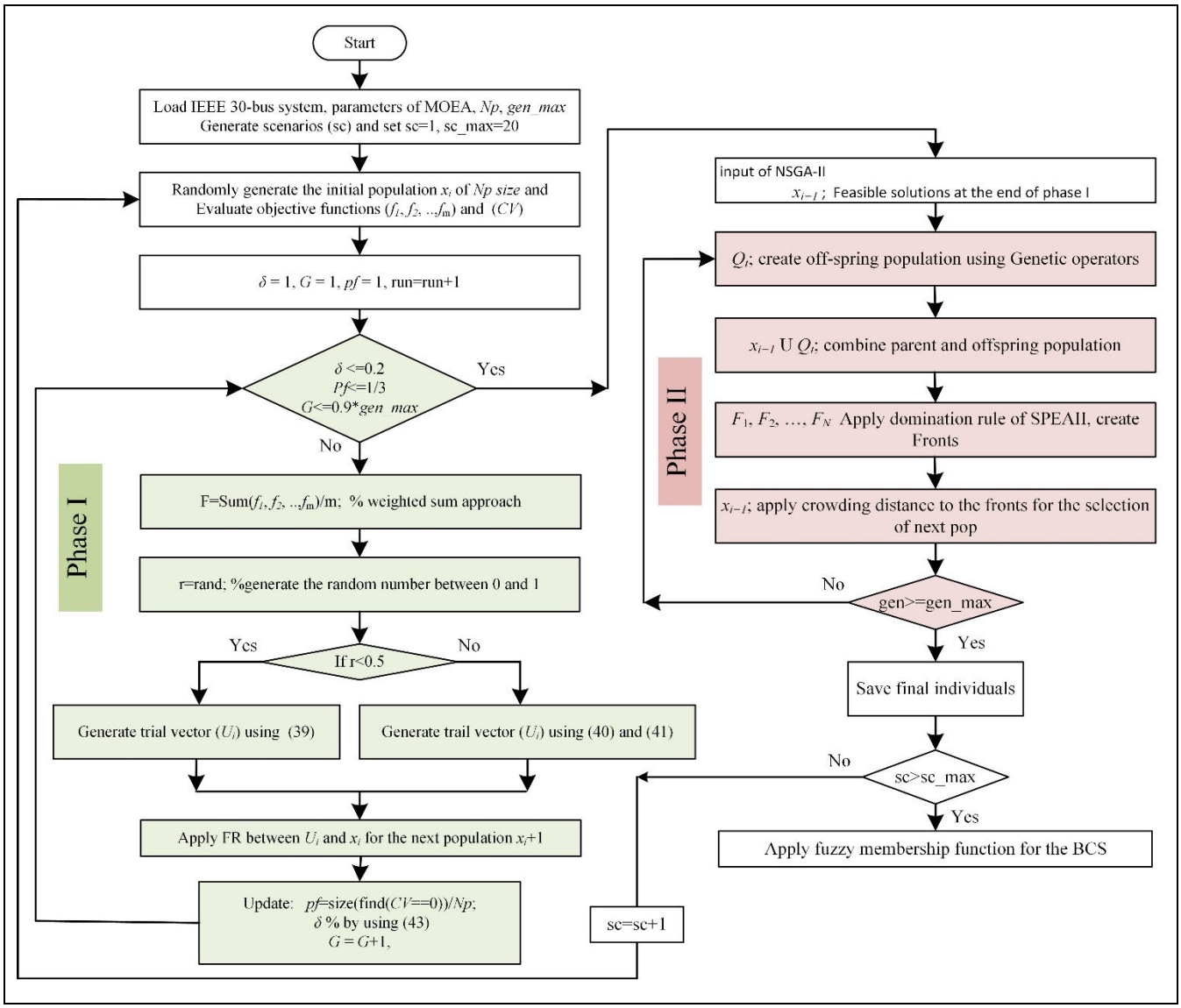

FIGURE 4. Flow chart of proposed algorithm.

mentioned above is continued until terminating criteria are satisfied. The steps of the second phase are given in the flow chart shown in Figure 4.

IV. SIMULATION RESULTS AND DISCUSSION

To implement the proposed formulation, the IEEE 30-bus network is considered to find the optimal solution to the PMO-ORPD problem by injecting wind and solar power. The proposed network has six units, nine shunt synchronous condensers, and four transformers. Bus, branch, and generator data are taken from [45], and the parameters for calculating cost functions are shown in Table 10 and 11 of Appendix A.

In the following subsequent subsections, simulation results and their detailed analysis and comparison are considered to investigate the effectiveness and performance of the proposed algorithm to solve deterministic and probabilistic MO-ORPD problems along with the integration of wind and solar generation. A deterministic MOORPD problem (without wind and solar) is considered to compare the proposed algorithm with the recently implemented methods. In the deterministic case, three recent constrained MOEA such as constrained co-evolutionary multi-objective optimization (CCMO) [46], ToP [47], and constrained two evolutionary archives algorithm (CTAEA) [48] and one former NSGAII [49] methods are implemented and select the best MOEA for the solution of PMO-ORPD problem.

A. DETERMINISTIC MO-ORPD

The control variables for the system include the voltage level of all generators, transformer tap ratio, and shunt VAR injections. These variables are continuous (generator's power and

voltages) and discrete (tap ratio of transformer and shunt VAR injection). For the fair composition between the implemented algorithms and recent methods available in the literature, all the control variables are considered continuous as well as mixed-integer in the base case. Each case is run 25 times independently, 25 Pareto fronts are obtained and the best P.F. is selected by using statistical data of hyper-volume (H.V.) performance indicator. To make a fair comparison of the different cases, the values of objective functions vary, so they are first normalized to ensure a uniform range between 0 and 1. A reference point of $(1, 1,\ldots,1)^{\mathrm{M}}$ is then used to compute the hyper-volume indicator (HVI). When comparing the P.F.s of different algorithm runs, the P.F. with the highest HVI value attained by the algorithm is considered the most optimal. For those interested in H.V. consider the reference [50].

The fuzzy decision-making (FDM) theory is used to choose the P.F.s of compromise solution [51]. The fuzzy set theory's membership function is explained as;

$$\mu_m^k = \begin{cases} 1 & for f_m^k \le f_m^{min} \\ \dfrac{f_m^{max} - f_m^k}{f_m^{max} - f_m^{min}} & for f_m^{min} < f_m^k < f_m^{max} \\ 0 & for f_m^k \ge f_m^{max} \end{cases} \tag{44}$$

where, f_m^k is the objective function, m is the index of objective functions, k is the nondominated solution, μ_m^k is membership function. Normalized membership (μ^k) function is computed by

$$\mu^k = \frac{\Sigma_{m=1}^{M} \mu_m^k}{\Sigma_{k=1}^{N_d} \Sigma_{m=1}^{M} \mu_m^k} \tag{45}$$

Out of all non-dominated solutions (N_d), a larger value of μ^k is the best compromise solution. Table 2 shows the statistical-value of H.V. of all the implemented algorithms and the BCS using FDM theory.

From Table 2, simulation results of H.V. and BCS in both cases, ToP gives the best results compared to all the other algorithms. Table 2 reveals that the lowest loss obtained in Case 1 is 4.4129 MW, whereas the V.D. is 0.0894 p.u subject to satisfying all the constraints obtained by ToP.

Additionally, all decision variables are feasible. The decision-maker must carefully choose the best options because certain reactive power levels are close to the maximum value. The load bus voltage is also within a narrow range of acceptable limitations. Due to the system voltage level being forced to be close to unity, the second objective function will not result in under or over-voltage problems.

However, this could also impact generators or VAR compensating equipment to the point that they exceed their reactive capacity restrictions. Furthermore, the supply and compensation of reactive power in the power system depend on several other factors, such as the constant transmission line parameters, load bus voltage type, and location of the load. However, in this work, ToP, with the CDP constraint handling technique, finds the solution within a feasible search space where the reactive power supply must lie within a desirable limit. Figure 5 shows the final non-dominated solutions of the best P.F. of all the algorithms for both of the cases.

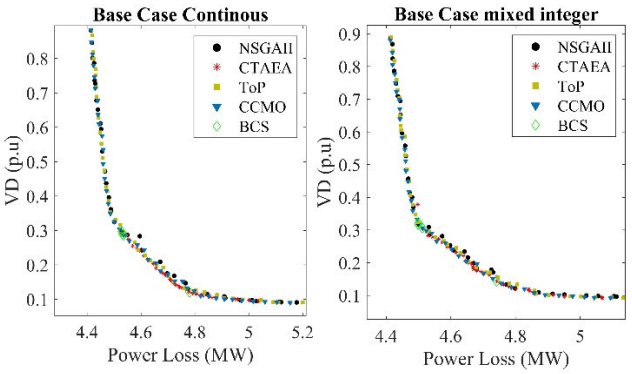

FIGURE 5. Best P.F. of all the algorithms and their B.C.

From Figure 5, it cannot be observed which MOEA gives the best P.F. in terms of both exploration and exploitation. Therefore, researchers used statistical tools such as H.V., min-max, the mean, and standard deviation to find the best MOEA. Further, the decision vector and objective functions of the best compromise solution are shown in Table 3. It can be observed from Table 3 that the decision variables are within the limit. The proposed algorithm efficiently finds the feasible non-dominated solutions of both problems, i.e., continuous and mixed integers. Likewise, Table 4 compares the proposed method with the recent methods available in the literature. From the comparative Table 4, ToP outperforms as compared to most of the algorithms in both of the objective functions.

The analysis and comparative study show that the ToP algorithm can find the most compromise solution compared to other recent optimization algorithms. Also, showing the values of H.V. and FDM results that the ToP outperforms as compared to all the other algorithms. It can be said that complex PMO-ORPD problems will be efficiently solved with the help of Top algorithms. In the next subsection, newly formulated problems of PMO-ORPD are solved with the help of the ToP algorithm.

B. PROBABILISTIC MO-ORPD (PMO-ORPD)

In this section, simulation studies are carried out to illustrate the proposed methodology for PMO-ORPD with integrating reactive capability of DFIG-based Wind and VSI-based solar PV. generation and system uncertainties.

In the PMO-ORPD problem, the proposed network is modified by replacing thermal generators at buses 5 & 8 with DFIG-based wind turbines (25 turbines of each 3MW) and VSI-based solar PV. (50 M.W. capacity) renewable generators. Furthermore, two classical formulations of simultaneous and four new formulations are designed considering the techno-economic of two and three objective functions. These are:

TABLE 2. The statistical value of H.V. of all the implemented algorithms and the BCS using FDM theory.

Continuous value of decision variable					FDM for the BCS					
Method	Max	Min	Mean	SD	index	f1	f2	mu	min f1	min f2
NSGAII	0.9158	0.5980	0.6234	0.0824	28	4.5286	0.2973	0.0295	4.4161	0.0911
CTAEA	0.7814	0.3018	0.7349	0.1201	39	4.7796	0.1213	0.0280	4.5266	0.0931
CCMO	0.8981	0.8907	0.8956	0.0025	28	4.5359	0.2868	0.0292	4.4141	0.0904
ToP	**0.9212**	**0.5492**	**0.8163**	**0.1650**	**38**	**4.5320**	**0.2891**	**0.0302**	**4.4129**	**0.0894**
Mixed-integer values of the decision variable					**FDM for the BCS**					
NSGAII	0.8812	0.8737	0.8771	0.0052	25	4.4995	0.3166	0.0297	4.4136	0.0969
CTAEA	0.7448	0.1122	0.5574	0.2504	27	4.7422	0.1432	0.0268	4.4982	0.0925
CCMO	0.8805	0.8758	0.8752	0.0031	24	4.5119	0.3065	0.0293	4.4131	0.0909
ToP	0.8871	0.8615	0.8806	0.0022	31	4.4991	0.3233	0.0299	4.4154	0.0932

TABLE 3. Simulation results of the base case of continuous and mixed integer type problems.

Parameters	Min	Max	NSGAII	CTAEA	ToP	CCMO	NSGAII	CTAEA	ToP	CCMO
V_1 (p.u.)	0.95	1.1	1.0675	1.0356	1.0620	1.0689	1.0676	1.0364	1.0661	1.0682
V_2 (p.u.)	0.95	1.1	1.0592	1.0260	1.0534	1.0589	1.0595	1.0276	1.0593	1.0589
V_5 (p.u.)	0.95	1.1	1.0340	1.0052	1.0319	1.0355	1.0357	1.0033	1.0366	1.0353
V_8 (p.u.)	0.95	1.1	1.0408	1.0051	1.0375	1.0370	1.0407	1.0087	1.0432	1.0403
V_{11} (p.u.)	0.95	1.1	1.0464	1.0355	1.0463	1.0325	1.0401	1.0364	1.0385	1.0355
V_{13} (p.u.)	0.95	1.1	1.0057	1.0141	1.0236	1.0117	1.0256	1.0231	1.0250	1.0155
T_{11} (p.u.)	0.9	1.1	4.9943	4.6114	0.8987	4.9980	5.00	2.80	4.60	5.00
T_{12} (p.u.)	0.9	1.1	2.6315	0.6334	3.6910	1.6833	0.20	2.00	2.80	2.20
T_{15} (p.u.)	0.9	1.1	4.7755	4.9979	4.8689	4.5745	4.00	4.80	4.00	5.00
T_{36} (p.u.)	0.9	1.1	4.9973	2.0961	4.2295	4.9137	5.00	4.80	5.00	5.00
QC_{10} (MVAr)	0	5	4.9947	4.9999	4.9029	4.9981	4.00	4.80	4.40	4.00
QC_{12} (MVAr)	0	5	4.8583	4.9792	4.9008	4.9953	5.00	4.80	5.00	5.00
QC_{15} (MVAr)	0	5	4.9761	5.0000	2.9527	4.6771	3.60	5.00	2.60	3.60
QC_{17} (MVAr)	0	5	5.0000	4.9998	4.8881	4.9996	5.00	5.00	5.00	4.80
QC_{20} (MVAr)	0	5	2.4162	2.3252	2.6784	2.4437	2.60	1.60	2.20	2.60
QC_{21} (MVAr)	0	5	1.0972	1.0514	1.0967	1.0984	1.10	1.06	1.10	1.10
QC_{23} (MVAr)	0	5	0.9775	0.9174	0.9428	0.9449	0.96	0.92	0.96	0.94
QC_{24} (MVAr)	0	5	1.0204	0.9970	1.0260	1.0224	1.02	1.02	1.02	1.02
QC_{29} (MVAr)	0	5	0.9997	0.9667	1.0001	1.0001	1.00	0.96	1.00	1.00
Ploss (M.W.)			**4.5286**	**4.7796**	**4.5320**	**4.5359**	**4.4995**	**4.7422**	**4.4991**	**4.5119**
VD (p.u.)			**0.2973**	**0.1213**	**0.2891**	**0.2868**	**0.3166**	**0.1432**	**0.3233**	**0.3065**
QG_1 (MVAr)	-20	150	87.9286	88.1796	87.9320	87.9359	87.8995	88.1422	87.8991	87.9119
QG_2 (MVAr)	-20	60	-0.6298	2.0338	-1.3786	3.8813	-1.4178	-1.2495	-4.8563	1.7724
QG_5 (MVAr)	-15	62.5	17.6294	14.8604	12.3037	15.9142	17.0869	14.8130	17.4422	15.3961
QG_8 (MVAr)	-15	48.7	23.6066	30.2139	26.6132	26.9598	25.1762	25.6823	25.5755	25.7533
QG_{11} (MVAr)	-10	40	29.2848	29.5963	31.1345	27.1749	28.5413	29.8726	32.1251	31.3346
QG_{13} (MVAr)	-15	44.7	23.5357	17.8391	23.3219	18.1268	20.5575	18.7110	19.7293	18.6081

TABLE 4. Comparison of simulation results of BCS of the proposed method with the recent literature.

Algorithm	P_{loss} (M.W.)	VD (p.u.)
ToP (continuous)	**4.5320**	**0.2891**
ToP (mixed integer)	4.4991	0.3233
MEAASS [52]	6.8893	0.3982
MODE [38]	4.8300	0.1204
OSAMGSA [36]	5.0713	0.1126
PSO [53]	5.3751	0.3651
NSGA-II [39]	6.7052	1.7366
QOTLBO [11]	5.2594	0.1210
CPVEIHBMO [27]	4.3783	0.6735
MOALO [28]	4.9818	0.3742
MOICA [29]	5.133	0.2811
QOTLBO [11]	6.4962	0.0856

- Classical formulation, C1: simultaneous minimization of EP_{Loss} and EVD
- Classical formulation, C2: simultaneous minimization of EP_{Loss} and EL_{index}
- Formulation 1— minimization of ETC_{Q_t} vs maximizes the $ERPR$
- Formulation 2— minimize the ETC_t vs maximizes the $ERPR$
- Formulation 3— minimization of ETC_{Q_t} vs. maximizes the $ERPR$ along with maximizing Q_{ch}
- Formulation 4 —minimization of ETC_{Q_t} vs. maximizes the $ERPR$ along with maximizing Q_{ch} vs. EL_{index}

Moreover, 1000 scenarios with the help of MCS are generated. Afterward, the fuzzy C-means (fcm) technique chooses the 20 representative scenarios, limiting the problem's complexity. Although the size of the representative set is very small as compared to the size of the probabilistic search space, it statistically guarantees a probability of 99.99% that at least one of the top 1% solutions will be in the 980 sample solutions. Furthermore, each scenario gives 40 non-dominated solutions, and from that, BCS is considered by applying FDM theory. Proposed scenarios are shown

TABLE 5. Proposed representative scenarios and their probabilities.

N_{sc}	% l	v (m/s)	p_{gW} (M.W.)	G (W/m^2)	p_{gS} (M.W.)	ρ_{sc}
SC1	0.892	7.186	24.153	168.838	8.442	0.133
SC2	0.893	4.912	11.030	518.068	25.903	0.020
SC3	**0.903**	**7.971**	**28.677**	**0.000**	**0.000**	**0.484**
SC4	0.908	5.061	11.893	1065.229	50.000	0.002
SC5	0.917	6.979	22.953	67.840	1.918	0.027
SC6	0.930	6.997	23.059	286.598	14.330	0.101
SC7	**0.941**	**0.977**	**0.000**	**229.156**	**11.458**	**0.036**
SC8	0.942	15.383	71.438	170.195	8.510	0.012
SC9	0.953	7.533	26.153	456.753	22.838	0.017
SC10	0.953	7.265	24.606	604.063	30.203	0.016
SC11	0.955	5.379	13.725	414.750	20.737	0.031
SC12	0.957	9.528	37.660	1117.755	50.000	0.001
SC13	0.959	8.039	29.069	353.788	17.689	0.040
SC14	0.960	8.021	28.965	669.115	33.456	0.012
SC15	0.966	3.258	1.488	963.829	48.191	0.042
SC16	0.968	8.447	31.424	755.848	37.792	0.004
SC17	0.970	1.726	0.000	1202.215	50.000	0.006
SC18	0.980	9.503	37.518	884.036	44.202	0.001
SC19	0.983	15.619	72.799	431.538	21.577	0.004
SC20	**1.047**	**16.199**	**75.000**	**253.267**	**12.663**	**0.011**

in Table 5; column six provides the probability of scenario, probability of scenario 3 is about 50% which shows the appearance of solar irradiance of half of a day. Table 5 clearly shows that in the same scenario, the maximum value of wind and solar PV. does not appear, and it is rarely in a realistic system.

Table 6 presents the simulation results of BCS solutions of all the objective functions. In Table 6 all the objective functions are minimized. However, maximization of RPR is done by minimization of -RPR. Table 6 shows that the maximum value of all the objective functions appears in sc7 and sc20, whereas a minimum value appears in sc1, sc4, and sc8. Therefore, extreme scenarios are 1, 4, 7, 8, and 20. Probability of each scenario ρ_{sc} from the last column of Table 5 and BCS of individual objective functions in Table 6 can be used to compute the expected values of objective functions as shown in Table 7.

In Table 7, bold values are the best values in the associated formulation. Comparing the simulation of four proposed formulations with the two classical formulations, we arrive at the following findings:

- The cost of active power generation is 743 $/h in both classical and proposed formulations is same. The cost of reactive power generation is optimal in the proposed formulation at 140 $/h compared to a classical formulation of 222.60 $/h in C1 and 226.04 $/h in C2. The cost of reactive power is minimal in a proposed formulation of 192 $/h compared to a classical formulation of 276 $/h. The overall cost of active and reactive power energy is minimum in the proposed formulation F4 which is 935.89 $/h, on the other hand, the energy cost in a classical formulation is about 1017.01 $/h. The cost of overall energy is minimal in the proposed formulation compared to the classical formulation because the cost of energy-producing devices is considered one of the objective functions in all four proposed formulations.
- The expected RPR is maximum in F4 proposed formulation, 283.23 MVAr, and minimum in C2, 264.6 MVAr.
- Expected power loss (EP_{Loss}) is minimum in C2, 5.223 MW, marginally less than the proposed formulation F4, 5.364 MW.
- The expected voltage deviation (V.D.) minimum in the C1 formulation is 0.296; after that minimum V.D. seen in formulation, F4 is 0.432. This paper's minimum load bus voltage is 0.95 p.u, whereas the maximum load bus voltage is 1.05 p.u. From these extreme voltage limits, aggregate V.D. is 1.2 p.u (24∗0.05=1.2, where 24 are load buses). In all the formulations, V.D. is less than 1.2 p.u.

L_{index} is minimum in C2 and F4 formulations which is 0.126 p.u. Line charging injection is maximum in C1 (18.044 MVAr), marginally better than F4, which is 17.948 MVAr.

- The average bus voltage is best in the F4 formulation, whereas the standard deviation (S.D.) is seen well in the C1 classical formulation.

The above remarks clearly show that if the system operator is interested in maximizing the ERPR and minimizing the expected cost of reactive power, the proposed formulation F4 gives better results than other formulations. Moreover, with the maximization of RPR, system dynamic voltage stability is also maximized because the generator's reactive power is the best source to control the voltage stability. For simplicity and better visibility, Pareto fronts (P.F.) of worst and best scenarios of formulation C1 and C2, sc1, sc4, and sc20 (extreme scenarios), are shown in Figure 6.

The red circle is the best compromise solution (BCS), computed using the fuzzy decision method. Figure 6 shows that

TABLE 6. Simulation results of BCS of all the formulation.

	C1		C2		F1		F2		F3		F4		
N_{sc}	P_{Loss}	VD	P_{Loss}	L_{index}	TC_{Q_t}	RPR	TC_t	RPR	TC_{Q_t}	$RPR + Q_{ch}$	TC_{Q_t}	$RPR + Q_{ch}$	L_{index}
SC1	**4.870**	**0.295**	**4.799**	**0.122**	**178.33**	**-288.58**	**904.12**	**-287.14**	**182.55**	**-303.17**	**179.50**	**-306.52**	**0.122**
SC2	4.933	0.316	4.861	0.122	179.36	-288.01	901.89	-288.08	182.86	-303.97	181.44	-304.01	0.123
SC3	5.255	0.291	5.180	0.125	188.56	-284.31	923.23	-284.66	184.64	-304.05	185.88	-303.93	0.124
SC4	**4.137**	**0.332**	**4.108**	**0.124**	**176.83**	**-288.68**	**893.53**	**-287.44**	**177.44**	**-304.62**	**180.27**	**-304.37**	**0.126**
SC5	5.837	0.289	5.748	0.127	195.93	-281.79	952.14	-279.21	202.02	-296.09	207.27	-296.54	0.126
SC6	5.316	0.292	**5.240**	**0.127**	**195.48**	**-282.05**	**946.23**	**-281.81**	199.70	-298.34	198.48	-298.05	0.128
SC7	**7.759**	**0.286**	**7.679**	**0.129**	**223.43**	**-272.34**	**1015.52**	**-270.82**	**231.80**	**-285.95**	**224.00**	**-290.43**	**0.130**
SC8	**3.184**	**0.193**	**3.040**	**0.129**	**177.01**	**-288.36**	**909.69**	**-285.66**	**176.79**	**-306.69**	**177.65**	**-304.98**	**0.130**
SC9	5.025	0.301	4.953	0.131	201.64	-278.52	958.31	-279.99	206.44	-294.25	202.31	-295.77	0.132
SC10	4.755	0.330	4.683	0.131	198.28	-280.53	951.12	-280.76	197.26	-298.94	198.35	-296.88	0.132
SC11	6.155	0.336	6.097	0.131	215.95	-274.54	986.06	-275.70	216.58	-292.04	214.54	-291.57	0.132
SC12	3.218	0.324	3.181	0.131	185.86	-284.57	920.05	-285.49	182.94	-303.46	188.95	-299.82	0.133
SC13	5.200	0.313	5.125	0.132	206.29	-276.00	974.18	-275.92	203.67	-296.83	204.21	-296.89	0.132
SC14	4.423	0.305	4.340	0.132	196.10	-281.09	954.51	-279.94	196.64	-297.27	197.42	-299.03	0.133
SC15	6.033	0.323	5.990	0.133	217.40	-272.67	989.54	-272.94	213.80	-292.70	219.66	-290.49	0.134
SC16	4.187	0.342	4.185	0.133	197.55	-280.69	955.64	-278.36	197.44	-296.96	196.54	-296.83	0.134
SC17	6.181	0.308	6.120	0.134	224.47	-269.96	991.06	-273.45	217.86	-291.61	224.20	-289.65	0.134
SC18	3.769	0.283	3.704	0.135	197.63	-280.69	955.15	-279.20	196.37	-298.91	195.61	-298.86	0.135
SC19	2.957	0.331	2.901	0.135	190.12	-283.16	944.54	-282.57	191.11	-298.05	188.55	-301.65	0.136
SC20	**4.296**	**0.276**	**4.159**	**0.145**	**229.33**	**-267.31**	**1027.01**	**-270.34**	**224.52**	**-287.50**	**227.21**	**-288.77**	**0.145**

TABLE 7. Expected values of objective functions and parameters for the formulations.

Performance	C1	C2	F1	F2	F3	F4
EC_{P_G} ($/h)	743.25	743.05	743.73	743.75	743.59	743.44
EC_{Q_G} ($/h)	222.60	226.04	141.21	141.00	140.08	**139.89**
EC_{L_t} ($/h)	7.424	**7.320**	7.666	7.676	7.594	7.518
$EC_{Q_{Ch}}$ ($/h)	4.402	**3.796**	5.958	5.958	5.958	5.942
C_{Ch} ($/h)	39.328	39.362	38.130	**38.059**	38.696	39.117
ETC_{Q_t} ($/h)	273.76	276.52	192.96	192.70	**192.32**	**192.47**
ETC_t ($/h)	1017.01	1019.57	936.69	936.44	935.91	**935.89**
ERPR (MVAr)	-264.94	-264.60	-282.66	-282.56	-282.98	**-283.23**
EP_{Loss} (M.W.)	**5.297**	**5.223**	5.470	5.476	5.418	5.364
EVD (p.u)	**0.296**	0.911	0.898	0.890	0.923	0.432
EL_{index} (p.u)	0.134	**0.126**	0.127	0.127	0.127	**0.126**
EQ_{ch} (MVAr)	18.044	**18.060**	17.495	17.462	**17.755**	17.948
Average bus voltage	1.0096	1.0383	1.0374	1.0366	**1.0369**	**1.0384**
SD of bus voltage	0.0023	0.0021	0.0058	0.0052	0.0049	0.0035

the proposed method finds the widely spread and converged P.F. Also, the P.F. of extreme scenarios for the formulations F1, F2, and F3 are shown in Figure 6. Due to high RPR, the proposed formulation ensures better power system stability and supports the voltage profile of the system at the time of contingency. Figure 6 clearly shows that the quality of obtained solutions most widely depends upon the load demand. With the increase in load demand, finding the uniform optimal solution that makes a trade-off between RPR and cost is very difficult. Therefore, the P.F.s of sc20 (at the load of 104%) in Figure 6 is discontinuous. Extreme scenarios of the final non-dominated solution of formulation F4 are shown in Figure 6. Formulation F4 gives a better voltage profile and L_{index} than all other formulations. Maximum expected RPR capacity is also obtained in this formulation F4. It is clear from the previously described figures that the suggested method may obtain a widely dispersed and complete P.F. for the decision-maker to select a single ideal option. Additionally, Figure 7 shows that all of the decision vectors are feasible. In Figure 7, each box plot shows the values of generator voltage, SVC, and transformer tap settings for all 20 scenarios.

Figure 8 shows the voltage profile and $L_{index}$of all the formulations sc20 (maximum load demand). All the variables are within the desirable limit. The proposed formulation's voltage stability index is slightly better than the classical one.

Figure 9 compares the expected total reactive power injection in all the formulations and the combined wind and solar integration share. It is observed from this Figure 9 that in both of the classical formulations, overall, all reactive power injection is a maximum of about 90 MVAr compared to the proposed formulation, which injects about 70 MVAr. It means that classical formulation will not be able to contribute to securing the power system if the load is increased or at the time of contingency appears. On the other hand, sufficient RPR is available in the proposed formulation to secure the system under load variation, and contingency occurred.

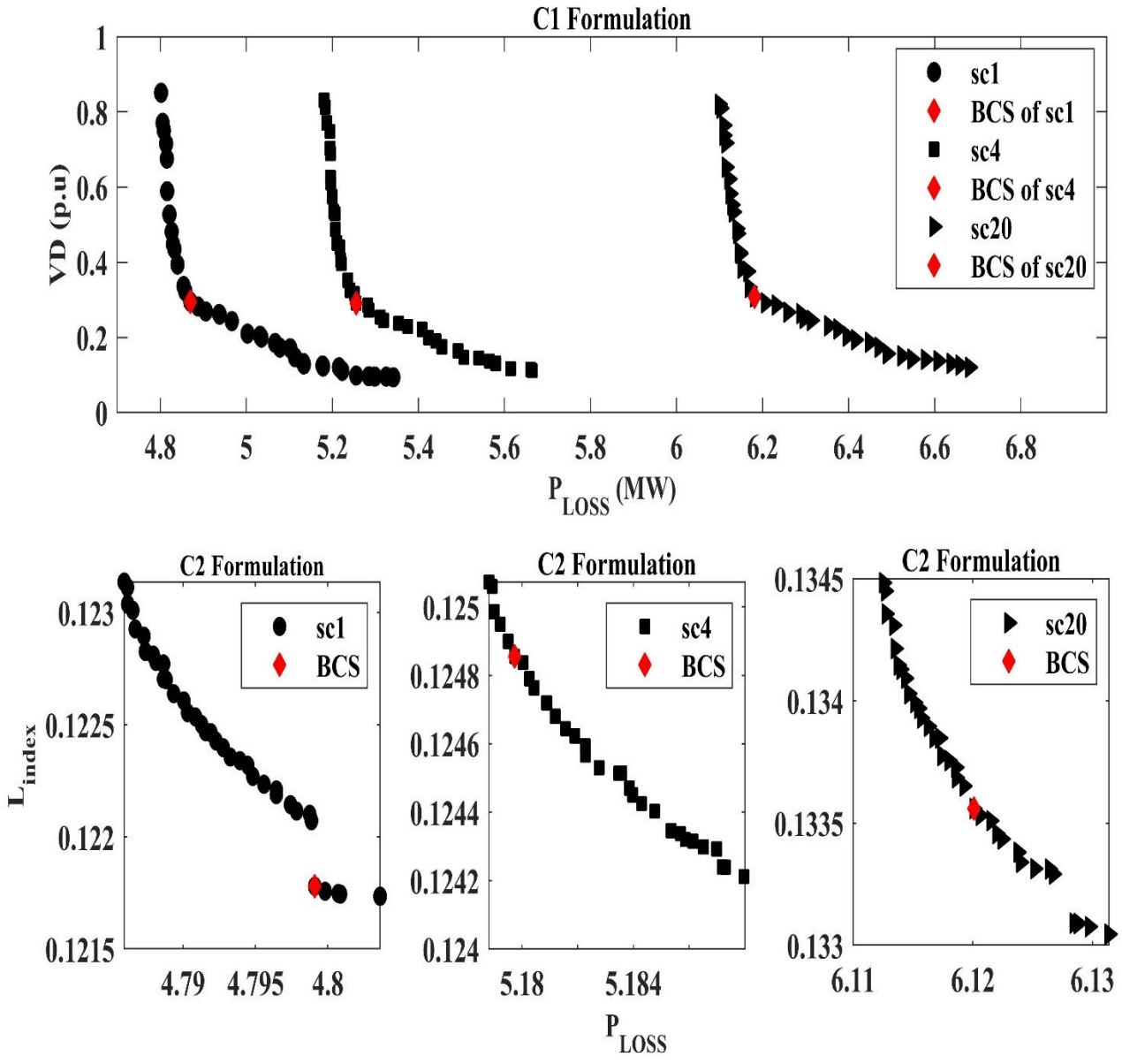

FIGURE 6. Final PF and BCS of extreme scenarios of formulation C1 and C2.

However, cumulative wind and solar injection are opposite to overall MVAr injection. Combined wind and solar share are minima in the classical formulation, whereas it is maximum injected in the proposed formulation. Therefore, wind and solar generation sufficiently support to increase in the *ERPR* of thermal generators. *ERPR* of thermal generators is the main source to respond to the variation in load demand and under fault conditions.

C. PROBABILISTIC MOOPRD ON 118BUS LARGE-SCALE POWER SYSTEM

To show the superiority and performance of the proposed algorithm, a large-scale 118-bus test system [54] is considered to solve the PMO-ORPD problem. This test system comprised 118 buses, 54 generators, and 216 transmission lines. Cumulative active and reactive power demand at 100% loading is 6787.2 MW and 2300.8 MVAr, respectively. It has nine transformers located at branches 9, 37, 42, 61, 107, 110, 119, 125, and 150 and fourteen shunt Var compensators installed at buses 5, 34, 37, 44, 45, 46, 48, 74, 79, 82, 83, 105, 107, and 110. In this work, IEEE 118-bus is modified as in [56] by injecting 12 wind generators at buses 1, 6, 9, 18, 19, 41, 43, 44, 62, 63, 72, and 80. The proposed test system has a reference generator located on bus 69. The single-line diagram of the IEEE 118-bus tests system is shown in Figure 10. Simulation results of two classical formulations (C1 and C2) and two proposed formulations (F1 and F2) are given in **Table** 8.

Expected cost of active power generation is varied due to uncertain wind integration. The expected cost of reactive

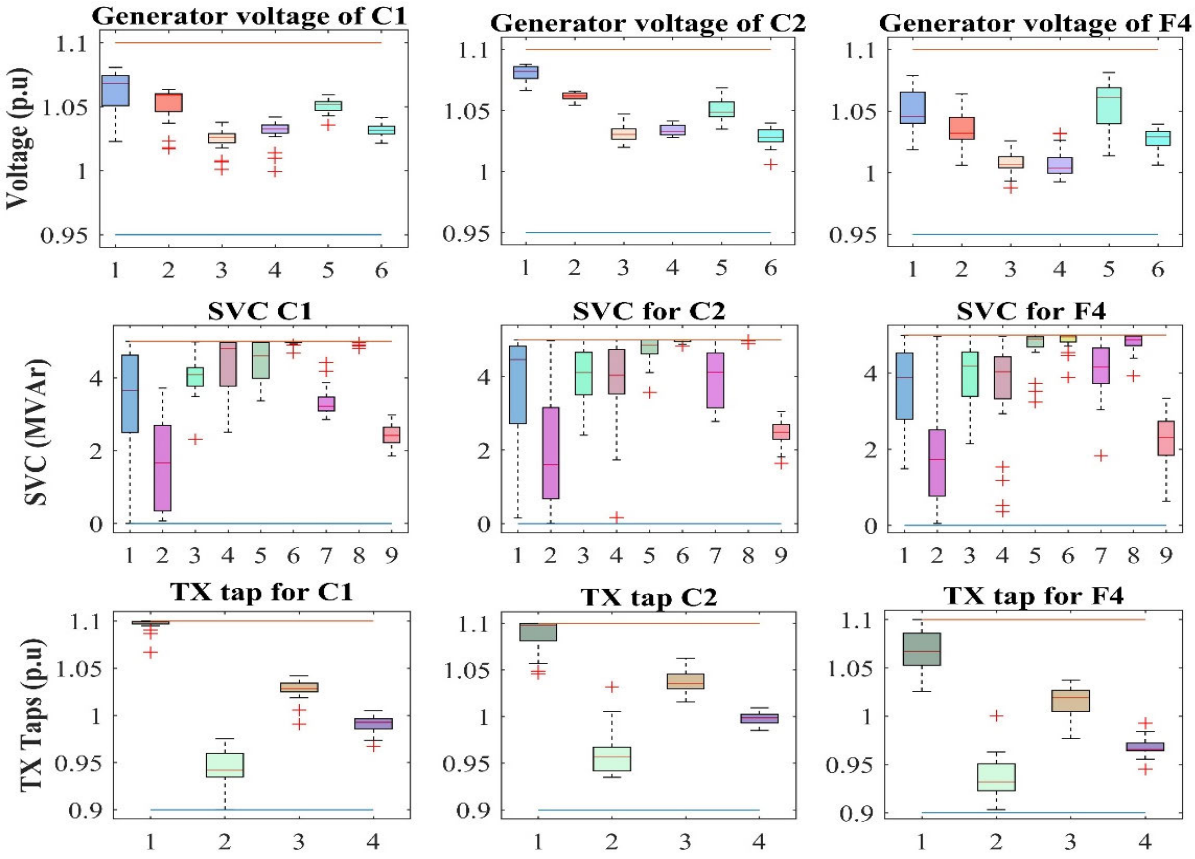

FIGURE 7. Box plot of generator voltage, SVC, and transformer tap settings of formulation C1, C2, and F4.

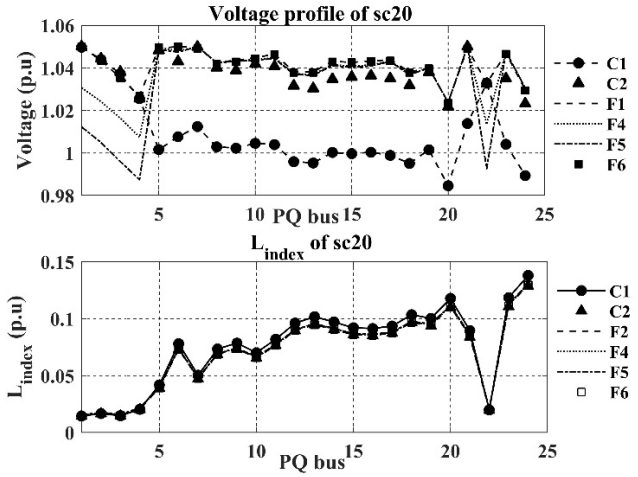

FIGURE 8. Voltage profile (p.u) and L_{index} of sc20 for all the formulations.

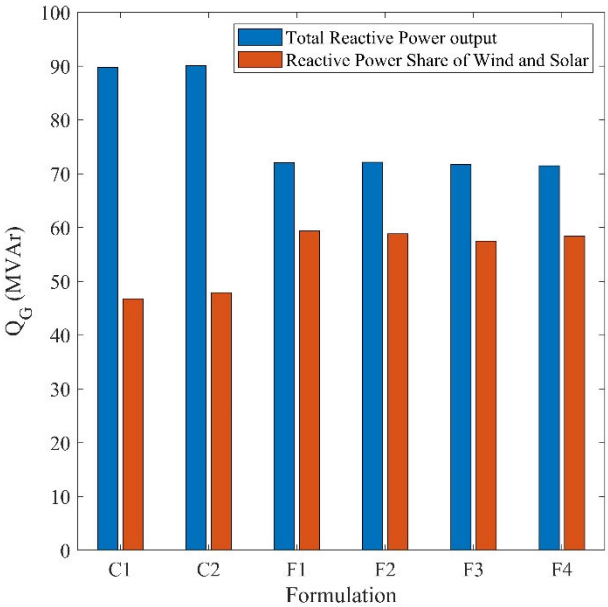

FIGURE 9. Comparison of total reactive power output and combined maximum share of wind and reactive solar power.

power generation is more than 50% less than classical formulations. Proposed formulations optimally inject MVAr into the system. Therefore, reactive power loss is marginally high compared to classical formulations. Expected reactive power reserve is approximately same in F, F2 and classical C1.

Simulation results in Table 8 demonstrate that the proposed formulation distributes the reactive power of generators optimally compared to classical formulations. The proposed formulation considers the impact of MVAR excitation across all the series and shunt components of the system. The final nondominated solutions of C1, C2, and F1, F2, are

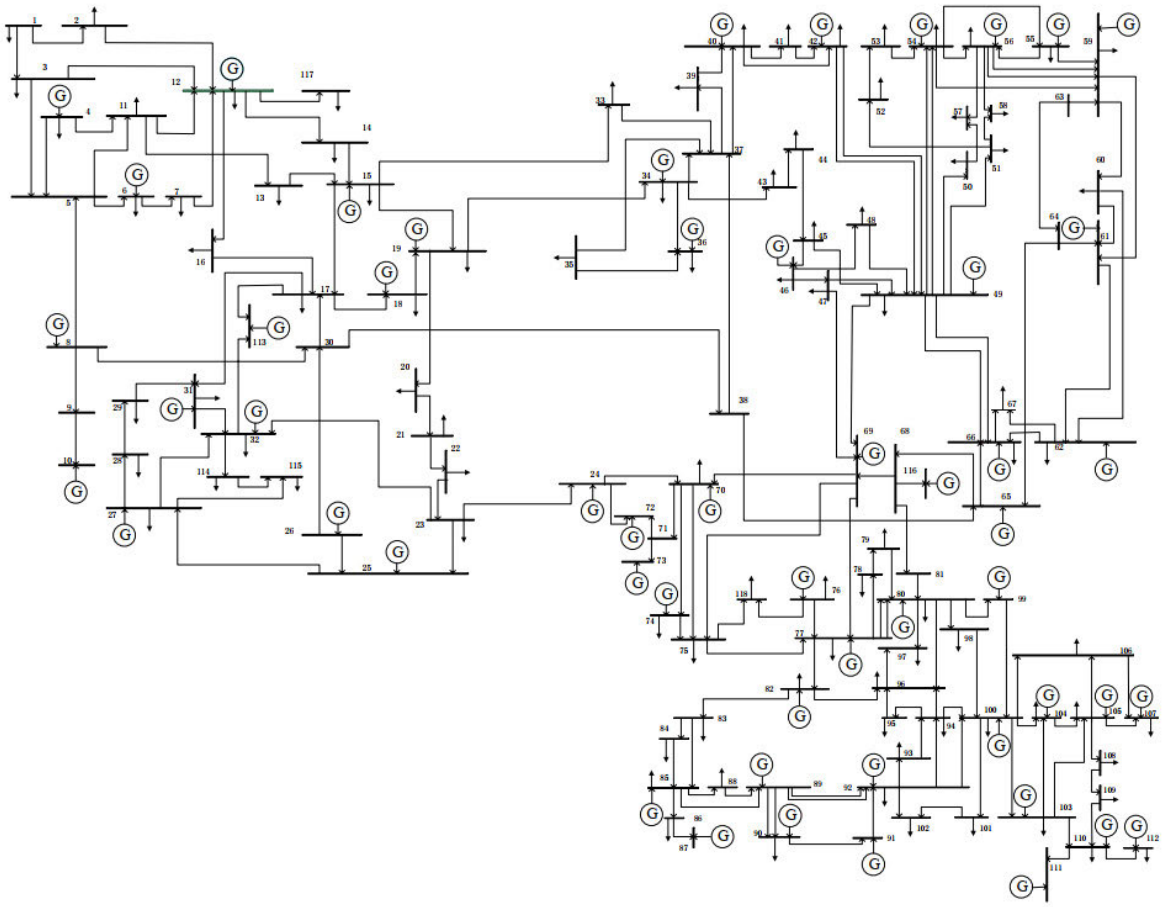

FIGURE 10. Proposed IEEE 118-bus system [54].

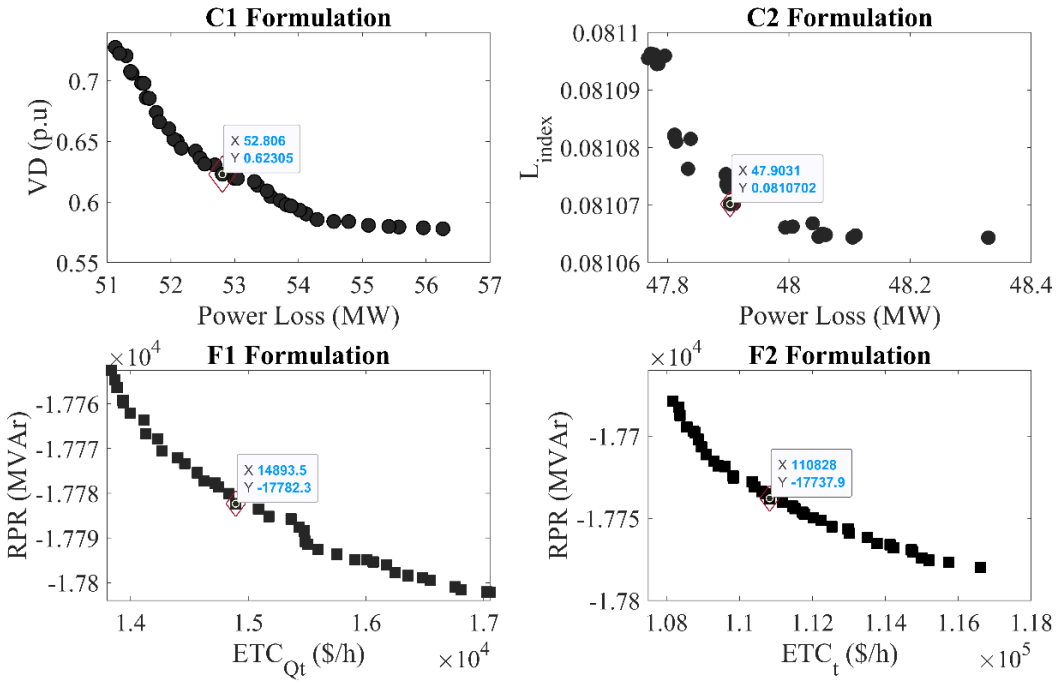

FIGURE 11. Final non-dominated solutions of IEEE 118-bus system.

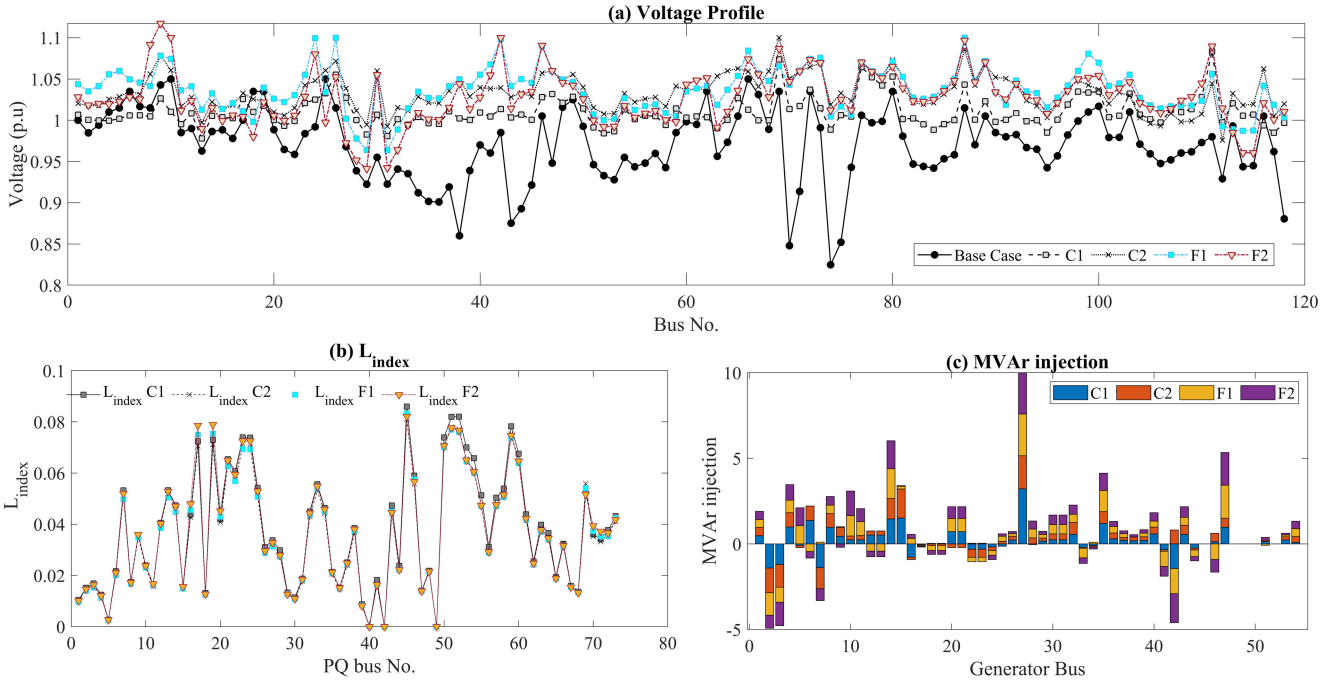

FIGURE 12. Comparison of voltage profile, L_{index}, and MVAr injection of C1, C2, and F1, F2.

TABLE 8. Expected values of objective functions and parameters for the formulations.

Performance	C1	C2	F1	F2
EC_{P_G} ($/h)	106038.3	107336.5	110412.5	94045.9
EC_{Q_G} ($/h)	26700.8	26480.7	10989.2	12928.2
EC_{L_t} ($/h)	594.7	546.7	672.2	629.1
$EC_{Q_{Ch}}$ ($/h)	6.380	6.706	9.228	8.692
C_{Ch} ($/h)	3009.0	3229.0	3222.8	3215.6
ETC_{Q_t} ($/h)	30311.0	30263.1	14893.4	16781.5
ETC_t ($/h)	136349.3	137599.7	125305.9	110827.5
ERPR (MVAr)	17642.1	17780.8	17782.3	17737.8
EP_{Loss} (M.W.)	52.805	47.903	57.374	63.111
EVD (p.u)	0.623	1.946	2.301	1.839
EL_{index} (p.u)	0.086	0.081	0.083	0.082
EQ_{ch} (MVAr)	1380.6	1481.5	1478.6	1475.3
Average bus voltage	1.003	1.025	1.027	1.016
SD of bus voltage	0.012	0.018	0.023	0.026

TABLE 9. Parameters of PDFs.

Uncertainty	PDF	Parameters	Power and load demand
Wind speed	Weibull	Shape, a=9; Scale, b=2	(75 M.W.) 25 turbines of each 3 M.W.
Solar irradiance	Lognormal	Mean, c=5.5; SD, d=0.5	Rated 50 MW
Load	Normal	Mean, μ_L=97; SD, σ_L=5	Percentage of load

shown in Figure 11. The figure shows the proposed algorithm finds the evenly distributed final nondominated solutions of conflicting objective functions. The best compromise solution is obtained by applying fuzzy weight decision-making. Figure 12 (a) compares the voltage profile of the base case and C1, C2, F1, and F2 of the 118-bus tests system. F1 found a better voltage profile than the base case, C2, and F2. Whereas, in terms of voltage profile, C1 outperforms. Table 8 elucidate that the proposed formulation outperforms C1 and C2 formulations. Furthermore, L_{index} of all P.Q. buses and MVAr injection of all the 54 generators of classical and proposed formulations are shown in Figure 12 (b)-(c).

TABLE 10. Minimum and maximum values of active and reactive power.

PV. bus #	Pgmax	Pgmin	Qmax	Qmin	PG
1	200	50	150	-20	Slack bus
2	80	20	60	-20	75
5	50	15	62.5	-15	40
5 (wind)	75	0	Variable	Variable	Variable
8	35	10	48.7	-15	30
8(Solar)	50	0	Variable	Variable	Variable
11	30	10	40	-10	25
13	40	12	44.7	-15	30

V. DISCUSSION

The multi-objective optimal reactive power dispatch (MO-RPD) problem is a significant research area in power systems engineering. It involves allocating reactive power among various devices in the power system to optimize multiple objectives simultaneously. Recent Extensive literature on ORPD is presented in Table 1, which integrates the main findings and limitations of various methodologies used in previous research to solve single and multi-objective ORPD problems. From Table 1, small IEEE 30-bus and large-scale 118-bus test systems are widely used in the literature.

Therefore, in this paper, the IEEE 30-bus and 118-bus tests system are considered to solve the ORPD problem.

TABLE 11. Constant parameters for the calculation of cost of thermal, wind and solar generators.

ai	bi	ci	aQ	bQ	cQ
0	2	0.00375	0	1.9998	0.037
0	1.75	0.0175	0	1.7499	0.0175
0	2.03	0	0	2.03	0
0	2.03	0	0	2.03	0
0	2.03	0	0	2.03	0
0	2.03	0	0	2.03	0
0	3	0.025	0	2.9976	0.025
0	3	0.025	0	2.9974	0.025

TABLE 12. Parameters for Qmax and Qmin of DFIG-based wind and VSI-based solar RES.

Parameters	Value (p.u)
Maximum rotor $\left(I_n^{rcwd}\right)$ and stator current $\left(I_n^{scwd}\right)$ of DFIG-based wind and rated inverter current $\left(I_n^{irpv}\right)$ of VSI-based solar PV.	1 p.u
Equivalent stator impedance of DFIG at bus i $\left(Z_i^s\right)$	0.0059+j0.1107
The equivalent main impedance of DFIG $\left(Z_i^m\right)$	j4.7351

At 100 MVA base and 135 base kV

Classically in the literature, as shown in Table 1, power loss, V.D., and stability index, L_{index} is frequently used to find the solution to ORPD problems. In this paper, these classical formulations are considered to compare the proposed algorithm with the available methods in the literature to show the superiority and performance of the proposed algorithm. Tables 3 and 4 elucidate that the proposed algorithm finds the approximate global optimal solution compared to other methods available in the literature in terms of Pareto Front (P.F.) and statistical comparison such (as maximum, minimum, and standard deviation values). Furthermore, hyper volume indicator (HVI) is used to compare the distribution and convergence of final non-dominated solutions of the proposed algorithm with the recent methods available in the literature.

Wind and solar power integration into the ORPD problem have gained significant attention in recent decades. As renewable energy sources, wind and solar power have unique characteristics that challenge their seamless integration into power systems. Several recent studies have focused on incorporating wind and solar power considerations into ORPD formulations to optimize the allocation of reactive power resources. Therefore, this paper integrates renewable energy source technologies with the proposed test systems, including DFIG-based wind generators and VSI-based solar PV. units. These probabilistic sources' reactive power capability constraints are shown in Fig. 2.

In the literature, load demand, wind, and solar power generation have all been modeled using normal, Weibull, and lognormal probability density functions (PDFs). One thousand MCS-based scenarios are generated using proposed PDFs. Practically, solutions to these scenarios are computationally expensive. Therefore scenario reduction technique based on distance metric has been employed to find the representative 20 scenarios, as shown in table 5.

In addition, we have introduced four new formulations for MO-RPD that aim to distribute reactive power optimally across all devices, considering the impact of uncertain wind and solar PV. generation. The mathematical derivation of these formulations is given in Section II, part C. These formulations consider all the devices that generate or absorb reactive power. Through applying these four formulations, we have demonstrated the effectiveness of our proposed approach in achieving optimal reactive power allocation and addressing the multiple objectives of power loss minimization, voltage stability enhancement, cost of reactive power generation, and maximizing reactive power reserve (RPR). The simulation results obtained from our formulation indicate significant improvements in system performance and validate the efficacy of our proposed methodologies. Introducing these new formulations for multi-objective optimal reactive power dispatch provides a comprehensive approach to address the challenges associated with reactive power allocation in power systems. By distributing reactive power optimally among all devices, we can achieve improved system efficiency, voltage stability, RPR, cost of MVAr injection, and integration of renewable energy sources.

VI. CONCLUSION

This paper formulated four new methodologies to solve the optimal reactive power dispatch (ORPD) problem. The proposed formulation considers the techno-economic objective functions, specifically the minimization of the active and reactive power cost, and the maximization of reactive power reserve. This leads to an effective solution to the probabilistic multi-objective ORPD (PMOORPD) problem, especially in the context of modern wind farms (WFs) and solar PV. The proposed formulations are necessary for effectively managing power systems with renewable energy sources and contribute to developing efficient and sustainable power systems. To validate the simulation results of the proposed algorithm, both continuous and mixed-integer deterministic study cases were analyzed and compared with the algorithms recently published in the literature. Fuzzy decision-making theory extracts the best compromise solution from the final non-dominated solutions.

Besides, an accurate reactive power capability curve of VSI-based solar PV. and DIFG-based wind turbines are considered to solve the classical and proposed formulation. To show the performance and effectiveness of the proposed techno-economic formulation, IEEE 30-bus and 118-bus test systems are modified to integrate wind and solar-based generation. Compared to the classical formulation, the proposed formulation effectively solves the PMO-ORPD problem to maximize expected RPR and minimize the expected active and reactive power costs. Integrating wind and solar-based reactive power into the power system can improve the Expected RPR and system stability in several ways. For example, it can help balance the reactive power demand and supply, reduce voltage fluctuations, and enhance the power system's ability to handle disturbances.

Additionally, integrating renewable energy sources can reduce the dependence on traditional sources of reactive power, such as synchronous generators, which can improve the power system's flexibility and resilience. Moreover, all the decision variables and constraints are within limits. In the future, IEEE 118 bus system is considered to implement active power reserve and commit or de-commitment of units by considering proposed formulations.

APPENDIX A

See Tables 9–12.

ACKNOWLEDGMENT

The authors extend their appreciation to the Deputyship for Research and Innovation, ''Ministry of Education'' in Saudi Arabia for funding this research (IFKSUOR3-261-1).

REFERENCES

[1] A. R. Abul'Wafa, ''Optimization of economic/emission load dispatch for hybrid generating systems using controlled elitist NSGA-II,'' *Electric Power Syst. Res.*, vol. 105, pp. 142–151, Dec. 2013, doi: 10.1016/j.epsr.2013.07.006.
[2] G. Fotis, V. Vita, and T. I. Maris, ''Risks in the European transmission system and a novel restoration strategy for a power system after a major blackout,'' *Appl. Sci.*, vol. 13, no. 1, p. 83, Dec. 2022, doi: 10.3390/app13010083.
[3] Y. Muhammad, R. Khan, M. A. Raja, F. Ullah, N. I. Chaudhary, and Y. He, ''Solution of optimal reactive power dispatch with FACTS devices: A survey,'' *Energy Rep.*, vol. 6, pp. 2211–2229, Nov. 2020.
[4] M. S. Saddique, A. R. Bhatti, S. S. Haroon, M. K. Sattar, S. Amin, I. A. Sajjad, S. S. Ul Haq, A. B. Awan, and N. Rasheed, ''Solution to optimal reactive power dispatch in transmission system using meta-heuristic techniques—Status and technological review,'' *Electric Power Syst. Res.*, vol. 178, Jan. 2020, Art. no. 106031, doi: 10.1016/j.epsr.2019.106031.
[5] M. De and S. K. Goswami, ''Optimal reactive power procurement with voltage stability consideration in deregulated power system,'' *IEEE Trans. Power Syst.*, vol. 29, no. 5, pp. 2078–2086, Sep. 2014, doi: 10.1109/TPWRS.2014.2308304.
[6] M. Ghaljehei, Z. Soltani, J. Lin, G. B. Gharehpetian, and M. A. Golkar, ''Stochastic multi-objective optimal energy and reactive power dispatch considering cost, loading margin and coordinated reactive power reserve management,'' *Electric Power Syst. Res.*, vol. 166, pp. 163–177, Jan. 2019, doi: 10.1016/j.epsr.2018.10.009.
[7] M. K. Mangoli, K. Y. Lee, and Y. Moon Park, ''Optimal real and reactive power control using linear programming,'' *Electric Power Syst. Res.*, vol. 26, no. 1, pp. 1–10, Jan. 1993, doi: 10.1016/0378-7796(93)90063-K.
[8] N. Grudinin, ''Reactive power optimization using successive quadratic programming method,'' *IEEE Trans. Power Syst.*, vol. 13, no. 4, pp. 1219–1225, 1998, doi: 10.1109/59.736232.
[9] S. K. Gupta, L. Kumar, M. K. Kar, and S. Kumar, ''Optimal reactive power dispatch under coordinated active and reactive load variations using FACTS devices,'' *Int. J. Syst. Assurance Eng. Manag.*, vol. 13, no. 5, pp. 2672–2682, Oct. 2022, doi: 10.1007/s13198-022-01736-9.
[10] A. A. A. El-Ela, A. M. Kinawy, R. A. El-Sehiemy, and M. T. Mouwafi, ''Optimal reactive power dispatch using ant colony optimization algorithm,'' *Electr. Eng.*, vol. 93, no. 2, pp. 103–116, Jun. 2011, doi: 10.1007/s00202-011-0196-4.
[11] B. Mandal and P. K. Roy, ''Optimal reactive power dispatch using quasi-oppositional teaching learning based optimization,'' *Int. J. Electr. Power Energy Syst.*, vol. 53, pp. 123–134, Dec. 2013, doi: 10.1016/j.ijepes.2013.04.011.
[12] M. Mehdinejad, B. Mohammadi-Ivatloo, R. Dadashzadeh-Bonab, and K. Zare, ''Solution of optimal reactive power dispatch of power systems using hybrid particle swarm optimization and imperialist competitive algorithms,'' *Int. J. Electr. Power Energy Syst.*, vol. 83, pp. 104–116, Dec. 2016.
[13] S. M. Shareef and R. S. Rao, ''Optimal reactive power dispatch under unbalanced conditions using hybrid swarm intelligence,'' *Comput. Electr. Eng.*, vol. 69, pp. 183–193, Jul. 2018.
[14] W. A. Misba, M. Ndoye, M. A. Arif, and G. V. Murphy, ''Multi-objective optimal reactive power dispatch using modified game theory,'' in *Proc. North Amer. Power Symp. (NAPS)*, Sep. 2017, pp. 1–6, doi: 10.1109/NAPS.2017.8107249.
[15] M. Basu, ''Quasi-oppositional differential evolution for optimal reactive power dispatch,'' *Int. J. Electr. Power Energy Syst.*, vol. 78, pp. 29–40, Jun. 2016, doi: 10.1016/j.ijepes.2015.11.067.
[16] P. P. Biswas, P. N. Suganthan, R. Mallipeddi, and G. A. J. Amaratunga, ''Optimal reactive power dispatch with uncertainties in load demand and renewable energy sources adopting scenario-based approach,'' *Appl. Soft Comput.*, vol. 75, pp. 616–632, Feb. 2019, doi: 10.1016/j.asoc.2018.11.042.
[17] M. Mahzouni-Sani, A. Hamidi, D. Nazarpour, and S. Golshannavaz, ''Multi-objective linearised optimal reactive power dispatch of wind-integrated transmission networks,'' *IET Gener., Transmiss. Distrib.*, vol. 13, no. 13, pp. 2686–2696, Jul. 2019.
[18] N. Habib Khan, R. Jamal, M. Ebeed, S. Kamel, H. Zeinoddini-Meymand, and H. M. Zawbaa, ''Adopting scenario-based approach to solve optimal reactive power dispatch problem with integration of wind and solar energy using improved marine predator algorithm,'' *Ain Shams Eng. J.*, vol. 13, no. 5, Sep. 2022, Art. no. 101726, doi: 10.1016/j.asej.2022.101726.
[19] L. Zhihuan, L. Yinhong, and D. Xianzhong, ''Non-dominated sorting genetic algorithm-II for robust multi-objective optimal reactive power dispatch,'' *IET Gener. Transmiss. Distrib.*, vol. 4, no. 9, pp. 1000–1008, 2010. [Online]. Available: https://digital-library.theiet.org/content/journals/10.1049/iet-gtd.2010.0105
[20] S. Ramesh, S. Kannan, and S. Baskar, ''An improved generalized differential evolution algorithm for multi-objective reactive power dispatch,'' *Eng. Optim.*, vol. 44, no. 4, pp. 391–405, Apr. 2012, doi: 10.1080/0305215X.2011.576761.
[21] K. Nuaekaew, P. Artrit, N. Pholdee, and S. Bureerat, ''Optimal reactive power dispatch problem using a two-archive multi-objective grey wolf optimizer,'' *Exp. Syst. Appl.*, vol. 87, pp. 79–89, Nov. 2017.
[22] M. Zhang and Y. Li, ''Multi-objective optimal reactive power dispatch of power systems by combining classification-based Multi-objective evolutionary algorithm and integrated decision making,'' *IEEE Access*, vol. 8, pp. 38198–38209, 2020, doi: 10.1109/ACCESS.2020.2974961.
[23] S. Jeyadevi, S. Baskar, C. K. Babulal, and M. Willjuice Iruthayarajan, ''Solving multiobjective optimal reactive power dispatch using modified NSGA-II,'' *Int. J. Electr. Power Energy Syst.*, vol. 33, no. 2, pp. 219–228, Feb. 2011, doi: 10.1016/j.ijepes.2010.08.017.
[24] A. Saraswat and A. Saini, ''Multi-objective optimal reactive power dispatch considering voltage stability in power systems using HFMOEA,'' *Eng. Appl. Artif. Intell.*, vol. 26, no. 1, pp. 390–404, Jan. 2013, doi: 10.1016/j.engappai.2012.06.008.
[25] G. Chen, L. Liu, P. Song, and Y. Du, ''Chaotic improved PSO-based multi-objective optimization for minimization of power losses and l index in power systems,'' *Energy Convers. Manag.*, vol. 86, pp. 548–560, Oct. 2014, doi: 10.1016/j.enconman.2014.06.003.
[26] J. P. Roselyn, D. Devaraj, and S. S. Dash, ''Multi objective differential evolution approach for voltage stability constrained reactive power planning problem,'' *Int. J. Electr. Power Energy Syst.*, vol. 59, pp. 155–165, Jul. 2014, doi: 10.1016/j.ijepes.2014.02.013.
[27] A. Ghasemi, K. Valipour, and A. Tohidi, ''Multi objective optimal reactive power dispatch using a new multi objective strategy,'' *Int. J. Electr. Power Energy Syst.*, vol. 57, pp. 318–334, May 2014, doi: 10.1016/j.ijepes.2013.11.049.
[28] S. Mouassa and T. Bouktir, ''Multi-objective ant lion optimization algorithm to solve large-scale multi-objective optimal reactive power dispatch problem,'' *COMPEL-Int. J. Comput. Math. Electr. Electron. Eng.*, vol. 38, no. 1, pp. 304–324, Jan. 2019.
[29] G. Chen, J. Cao, Z. Zhang, and Z. Sun, ''Application of imperialist competitive algorithm with its enhanced approaches for multi-objective optimal reactive power dispatch problem,'' *Eng. Lett.*, vol. 27, no. 3, pp. 579–592, 2019.
[30] B. Zhou, K. W. Chan, T. Yu, H. Wei, and J. Tang, ''Strength Pareto multigroup search optimizer for multiobjective optimal reactive power dispatch,'' *IEEE Trans. Ind. Informat.*, vol. 10, no. 2, pp. 1012–1022, May 2014, doi: 10.1109/TII.2014.2310634.
[31] S. M. Mohseni-Bonab and A. Rabiee, ''Optimal reactive power dispatch: A review, and a new stochastic voltage stability constrained multi-objective model at the presence of uncertain wind power generation,'' *IET Gener., Transmiss. Distrib.*, vol. 11, no. 4, pp. 815–829, Mar. 2017.
[32] S. M. Mohseni-Bonab, A. Rabiee, and B. Mohammadi-Ivatloo, ''Voltage stability constrained multi-objective optimal reactive power dispatch under load and wind power uncertainties: A stochastic approach,'' *Renew. Energy*, vol. 85, pp. 598–609, Jan. 2016, doi: 10.1016/j.renene.2015.07.021.

[33] T. M. Aljohani, A. F. Ebrahim, and O. Mohammed, "Single and multiobjective optimal reactive power dispatch based on hybrid artificial physics-particle swarm optimization," *Energies*, vol. 12, no. 12, p. 2333, Jun. 2019.

[34] M. U. Keerio, A. Ali, M. Saleem, N. Hussain, and R. Hussain, "Multi-objective optimal reactive power dispatch considering probabilistic load demand along with wind and solar power integration," in *Proc. 2nd Int. Conf. Smart Power Internet Energy Syst. (SPIES)*, Sep. 2020, pp. 502–507, doi: 10.1109/SPIES48661.2020.9243016.

[35] R.-H. Liang, J.-C. Wang, Y.-T. Chen, and W.-T. Tseng, "An enhanced firefly algorithm to multi-objective optimal active/reactive power dispatch with uncertainties consideration," *Int. J. Electr. Power Energy Syst.*, vol. 64, pp. 1088–1097, Jan. 2015, doi: 10.1016/j.ijepes.2014.09.008.

[36] T. Niknam, M. R. Narimani, R. Azizipanah-Abarghooee, and B. Bahmani-Firouzi, "Multiobjective optimal reactive power dispatch and voltage control: A new opposition-based self-adaptive modified gravitational search algorithm," *IEEE Syst. J.*, vol. 7, no. 4, pp. 742–753, Dec. 2013, doi: 10.1109/JSYST.2012.2227217.

[37] S. M. Mohseni-Bonab, A. Rabiee, B. Mohammadi-Ivatloo, S. Jalilzadeh, and S. Nojavan, "A two-point estimate method for uncertainty modeling in multi-objective optimal reactive power dispatch problem," *Int. J. Electr. Power Energy Syst.*, vol. 75, pp. 194–204, Feb. 2016, doi: 10.1016/j.ijepes.2015.08.009.

[38] A. H. Shojaei, A. A. Ghadimi, M. R. Miveh, F. Mohammadi, and F. Jurado, "Multi-objective optimal reactive power planning under load demand and wind power generation uncertainties using ε-constraint method," *Appl. Sci.*, vol. 10, no. 8, p. 2859, Apr. 2020, doi: 10.3390/app10082859.

[39] Z. Li, Y. Li, and X. Duan, "Multiobjective optimal reactive power flow using elitist nondominated sorting genetic algorithm: Comparison and improvement," *J. Electr. Eng. Technol.*, vol. 5, no. 1, pp. 70–78, Mar. 2010.

[40] T. Moger and T. Dhadbanjan, "Fuzzy logic approach for reactive power coordination in grid connected wind farms to improve steady state voltage stability," *IET Renew. Power Gener.*, vol. 11, no. 2, pp. 351–361, Feb. 2017, doi: 10.1049/iet-rpg.2016.0119.

[41] K. Zou, A. P. Agalgaonkar, K. M. Muttaqi, and S. Perera, "Distribution system planning with incorporating DG reactive capability and system uncertainties," *IEEE Trans. Sustain. Energy*, vol. 3, no. 1, pp. 112–123, Jan. 2012, doi: 10.1109/TSTE.2011.2166281.

[42] J. W. Lamont and J. Fu, "Cost analysis of reactive power support," *IEEE Trans. Power Syst.*, vol. 14, no. 3, pp. 890–898, Aug. 1999, doi: 10.1109/59.780900.

[43] A. J. Conejo, J. M. Arroyo, N. Alguacil, and A. L. Guijarro, "Transmission loss allocation: A comparison of different practical algorithms," *IEEE Trans. Power Syst.*, vol. 17, no. 3, pp. 571–576, Aug. 2002, doi: 10.1109/TPWRS.2002.800894.

[44] E. Zitzler, M. Laumanns, and L. Thiele, "SPEA2: Improving the strength Pareto evolutionary algorithm," Tech. Rep., 103, 2001.

[45] R. D. Zimmerman, C. E. Murillo-Sanchez, and R. J. Thomas, "MATPOWER: Steady-state operations, planning, and analysis tools for power systems research and education," *IEEE Trans. Power Syst.*, vol. 26, no. 1, pp. 12–19, Feb. 2011, doi: 10.1109/tpwrs.2010.2051168.

[46] Y. Tian, T. Zhang, J. Xiao, X. Zhang, and Y. Jin, "A coevolutionary framework for constrained multiobjective optimization problems," *IEEE Trans. Evol. Comput.*, vol. 25, no. 1, pp. 102–116, Feb. 2021.

[47] Z. Liu and Y. Wang, "Handling constrained multiobjective optimization problems with constraints in both the decision and objective spaces," *IEEE Trans. Evol. Comput.*, vol. 23, no. 5, pp. 870–884, Oct. 2019, doi: 10.1109/TEVC.2019.2894743.

[48] K. Li, R. Chen, G. Fu, and X. Yao, "Two-archive evolutionary algorithm for constrained multiobjective optimization," *IEEE Trans. Evol. Comput.*, vol. 23, no. 2, pp. 303–315, Apr. 2019, doi: 10.1109/TEVC.2018.2855411.

[49] K. Deb, A. Pratap, S. Agarwal, and T. Meyarivan, "A fast and elitist multiobjective genetic algorithm: NSGA-II," *IEEE Trans. Evol. Comput.*, vol. 6, no. 2, pp. 182–197, Apr. 2002, doi: 10.1109/4235.996017.

[50] L. While, P. Hingston, L. Barone, and S. Huband, "A faster algorithm for calculating hypervolume," *IEEE Trans. Evol. Comput.*, vol. 10, no. 1, pp. 29–38, Feb. 2006, doi: 10.1109/TEVC.2005.851275.

[51] H. Pulluri, R. Naresh, and V. Sharma, "An enhanced self-adaptive differential evolution based solution methodology for multiobjective optimal power flow," *Appl. Soft Comput.*, vol. 54, pp. 229–245, May 2017, doi: 10.1016/j.asoc.2017.01.030.

[52] L. Hongxin, L. Yinhong, and C. Jinfu, "Adaptive multiple evolutionary algorithms search for multi-objective optimal reactive power dispatch," *Int. Trans. Electr. Energy Syst.*, vol. 24, no. 6, pp. 780–795, Jun. 2014, doi: 10.1002/etep.1730.

[53] N. Mancer, B. Mahdad, and K. Srairi, "Multi objective optimal reactive power flow based STATCOM using three variant of PSO," *Int. J. Energy Eng.*, vol. 2, no. 2, pp. 1–7, Apr. 2012.

[54] I. Peña, C. B. Martinez-Anido, and B. Hodge, "An extended IEEE 118-bus test system with high renewable penetration," *IEEE Trans. Power Syst.*, vol. 33, no. 1, pp. 281–289, Jan. 2018, doi: 10.1109/TPWRS.2017.2695963.

AAMIR ALI received the B.E., M.E., and Ph.D. degrees in electrical engineering from the Quaid-e-Awam University of Engineering Science and Technology (QUEST), Nawabshah, Sindh, Pakistan. He is currently an Assistant Professor with the Department of Electrical Engineering, QUEST. His main research interests include power system optimization, grid-connected and islanded operation of distributed generation, smart grids, and multi-objective evolutionary algorithms.

GHULAM ABBAS received the B.Eng. degree in electrical engineering from QUEST, Nawabshah, Pakistan, in 2017, and the M.Eng. degree in electrical engineering from Southeast University, Nanjing, China, in 2019, where he is currently pursuing the Ph.D. degree in electrical engineering. His research interests include distributed generations' integration, planning, and optimization.

MUHAMMAD USMAN KEERIO was born in Nawabshah, Pakistan, in December 1965. He received the bachelor's degree in electrical (power) engineering from the Mehran University of Engineering and Technology, Jamshoro, in 1991, the master's degree in control engineering from NUST, Karachi, in 2002, and the Ph.D. degree in controls and robotics from the Beijing Institute of Technology, China, in 2008. His research interests include electrical and control engineering, curriculum development, institutional accreditation, neural networks, and optimization.

EZZEDDINE TOUTI received the B.S. degree in electrical engineering from the Higher National College of Engineers of Tunis, Tunisia, in 1997, the master's degree in electrical engineering from the National College of Engineers of Tunis, Tunisia, in 2005, and the Ph.D. degree in induction generators wind turbine, power quality and electric drives from the National College of Engineers of Monastir, Tunisia, and Artois University, France, in 2013. In 2005, he joined the Laboratory of Industrial Systems Engineering and Renewable Energies (LISIER), University of Tunis, Tunisia, as a Researcher Faculty Member. He is currently an Associate Professor with the College of Engineering, Northern Border University. His research interests include renewable energy, smart grids, electric vehicle, power electronics, and control of electrical systems.

ZAHOOR AHMED is currently a Professor with the Department of Electrical Engineering, Balochistan University of Engineering and Technology Khuzdar, Khuzdar, Pakistan. He has over 20 research publications in national and international journals and conferences. His research interests include distributed generations' integration, planning, and optimization.

OSAMAH ALSALMAN received the B.S. degree from King Saud University (KSU), the M.Sc. degree from University of Michigan–Ann Arbor, and the Ph.D. degree in electrial and electronic engineering from The University of Manchester. Currently, he is an Assistant Professor with the Electrial Engineering Department of College of Engineering, King Saud University, Saudi Arabia. His research interest includes renewable energy, electronics and optoelectronics.

YUN-SU KIM (Senior Member, IEEE) received the B.S. and Ph.D. degrees in electrical engineering from Seoul National University, Seoul, South Korea, in 2010 and 2016, respectively. He was a Senior Researcher with the Korea Electrotechnology Research Institute (KERI), from 2015 to 2017. He joined the Gwangju Institute of Science and Technology (GIST), as a Faculty Member, in 2018, where he is currently an Associate Professor with the Graduate School of Energy Convergence. His research interests include distribution networks, distributed energy resources, microgrids, and artificial intelligence. He was the Director of the Korean Society for New and Renewable Energy and the Korean Institute of Electrical Engineers.